Biophysical Journal
Article

Biophysical Society

Volume Transitions of Isolated Cell Nuclei Induced by Rapid Temperature Increase

Chii J. Chan,[1,2,*] Wenhong Li,[2] Gheorghe Cojoc,[2] and Jochen Guck[1,2,*]
[1]Cavendish Laboratory, Department of Physics, University of Cambridge, Cambridge, United Kingdom; and [2]Biotechnology Center, Technische Universität Dresden, Dresden, Germany

ABSTRACT Understanding the physical mechanisms governing nuclear mechanics is important as it can impact gene expression and development. However, how cell nuclei respond to external cues such as heat is not well understood. Here, we studied the material properties of isolated nuclei in suspension using an optical stretcher. We demonstrate that isolated nuclei regulate their volume in a highly temperature-sensitive manner. At constant temperature, isolated nuclei behaved like passive, elastic and incompressible objects, whose volume depended on the pH and ionic conditions. When the temperature was increased suddenly by even a few degrees Kelvin, nuclei displayed a repeatable and reversible temperature-induced volume transition, whose sign depended on the valency of the solvent. Such phenomenon is not observed for nuclei subjected to slow heating. The transition temperature could be shifted by adiabatic changes of the ambient temperature, and the magnitude of temperature-induced volume transition could be modulated by modifying the chromatin compaction state and remodeling processes. Our findings reveal that the cell nucleus can be viewed as a highly charged polymer gel with intriguing thermoresponsive properties, which might play a role in nuclear volume regulation and thermosensing in living cells.

INTRODUCTION

The nucleus is the largest organelle in eukaryotic cells, easily occupying about half of the volume of the cell. It is the site of major cellular functions such as DNA replication, transcriptional regulation, and ribosome assembly. Its mechanical stiffness and coupling to the cytoskeleton are crucial in sustaining the structural and functional integrity of a cell. Changes in nuclear shape and volume might alter nuclear protein concentration and gene expression, and affect development in normal functions and diseases (1,2). Extensive studies in the past have shown that the nucleus is relatively stiff compared to the cytoplasm (3–5), and displays a power-law rheology (6). Nuclear stiffness depends largely on the nuclear lamina, and changes in the expression of lamin A/C during stem cell differentiation can regulate the physical plasticity of the nucleus and impact matrix-directed differentiation (2,7). Recently, chromatin, a major component of nuclear architecture, has also been implicated to impact nuclear mechanics. Studies on isolated nuclei showed that histone tail-tail interactions counter the outward entropic pressure of the DNA, and enzymatic disruption of these interactions can lead to chromatin decondensation and nuclear softening (8). Compressive studies on nuclei in situ showed that chromatin decondensation induced nuclear softening of up to 50% (9). Chromatin compaction is also pertinent in embryonic development: Chalut et al. (10) showed that the nuclear stiffness of mouse embryonic stem cells devoid of lamin A/C is correlated with chromatin condensation regulated by transcriptional machinery. Notably, a particular transition state of these embryonic stem cells can exhibit interesting mechanical properties such as auxeticity, which is likely driven by chromatin decondensation (11). These studies provide emerging evidence supporting the role of chromatin organization in regulating nuclear shape changes and functions.

While the mechanical aspects of cell nuclei have been extensively studied, less is known about nuclear mechanical stability in response to transient or long-time temperature changes. DNA polymers have been shown to be relatively stable against heat at physiological temperatures (12), keeping their double-stranded shape up to a melting temperature of 70°C. DNA is therefore more thermoresistant than most proteins in the cell, which often denature above 40°C (13). Other studies report a highly thermolabile nuclear matrix that is sensitive to thermal shock (14). Recent studies showed

Submitted August 9, 2016, and accepted for publication January 17, 2017.

*Correspondence: chii.chan@embl.de or jochen.guck@tu-dresden.de

Chii J. Chan's present address is European Molecular Biology Laboratory, Heidelberg, Germany.

Wenhong Li's present address is Weizmann Institute of Science, Rehovot, Israel.

Editor: Gijsje Koenderink.

http://dx.doi.org/10.1016/j.bpj.2017.01.022

© 2017 Biophysical Society.

This is an open access article under the CC BY-NC-ND license (http://creativecommons.org/licenses/by-nc-nd/4.0/).

that nuclei in suspended cells undergo intriguing restructuring and shape remodeling in response to temperature increase above physiological temperatures (15). In the nucleus, various electrostatic interactions are at play: the chromatin fibers comprising of negatively charged chains of DNA-histone complex (nucleosomes) are surrounded by a sea of positively charged counterions that effectively screen the negative repulsions between DNA segments (16). The competition between electrostatics and entropy govern the large-scale chromatin organization (17). Multivalent salts can even induce a net attractive interaction between chromatin fibers, leading to chromatin hypercondensation (18). In soft matter physics, such polyelectrolyte gels are known to be thermoresponsive, that is, they display volume transitions in response to temperature changes. Thermomechanical studies of cell nuclei may therefore inform models of living organelles as complex materials with interesting material properties.

In this work, we studied how isolated nuclei in vitro respond to mechanical stress and transient heat, in various ionic conditions and chromatin-perturbed states. Using an optical stretcher (OS) operating at 780 nm (a contact-free technique that incurs minimal heating), we find that at constant temperature and in monovalent salts, isolated nuclei behave as passive elastic and incompressible objects. We further demonstrate that with a sudden increase in temperature of only a few degrees of Kelvin, cell nuclei can display reversible and repeatable volume transitions, whose magnitude depends on the rate of temperature increase and ionic conditions. Histone interactions and chromatin remodeling processes also play an important role in regulating nuclear mechanical susceptibility against such temperature-induced volume transitions. Overall, our work provides evidence that isolated cell nuclei share similar physical attributes as polyelectrolyte gels, which may advance our biological understanding of nuclear volume regulation in living cells.

MATERIALS AND METHODS

Nuclei preparation

The nuclear isolation protocol was adapted and modified from previous work (19–21). Cell nuclei were extracted from whole cells via chemical means. Six milliliters of HL60 cells (~1,000,000/mL) were centrifuged at 4°C, 800 rpm for 5 min, and washed with cold PBS (4°C). The cells were then resuspended in a hypotonic buffer containing 10 mM HEPES (pH 7.5), 1 mM DL-Dithiothreitol (Sigma-Aldrich, St. Louis, MO), and protease inhibitor (1 tablet per 10 mL; Roche, Basel, Switzerland), and incubated on ice for 10 min to allow for swelling. IGEPAL solution (nonionic detergent; Sigma-Aldrich) and citric acid were then added to a final concentration of 0.1% and 1 mM, respectively. The solution was quickly vortexed for 10 s, before being centrifuged at 4°C for 5 min at 1000 rpm. A clean nuclei pellet should be visible at this stage. The solution was then resuspended in 4°C PBS and washed once more with cold PBS to wash out any residual effects of IGEPAL and citric acid.

To monitor nuclear volume changes in different pH, HL60 nuclei were suspended in PBS (pH 7.5) with pH adjusted by the addition of HCl or NaOH. For experiments on changing ionic conditions, nuclei were resuspended in PBS of various diluting ratio: 0% (deionized water), 1, 5, 10, 20, 50, and 100% PBS. Monovalent salts such as NaCl and KCl were tested at 10, 100, and 300 mM. To condense the nuclei, several multivalent salts were used: $[Co(NH_3)]Cl_3$ at 0.01 and 0.1 mM, $CaCl_2$, and $MgCl_2$ at 0.01, 0.1, 1, and 10 mM. To effect fragmentation of chromatin structures, both 0.1 and 0.01 mg/mL of deoxyribonuclease I (D5025; Sigma-Aldrich) were used. To decondense chromatin by histone modifications, clostripain (Sigma-Aldrich) or trichostatin A (TSA; Millipore, Billerica, MA) were used. Clostripain was first dissolved in a buffer containing 1 mM $CaCl_2$, 2.5 mM DL-Dithiothreitol, and 5% PBS, to a final concentration of 4 mU/μL. Solution was then kept at room temperature for 3 h for activation to take place, before being added to isolated nuclei. For TSA experiments, HL60 cells were incubated with 300 nM TSA in cell culture medium for 11 h in a cell incubator before assaying. TSA was kept in the medium during OS experiments to avoid reversible effects of the drug (22).

For chromatin remodeling experiments, dexrazoxane or ICRF-187 (D1446; Sigma-Aldrich), an inhibitor of topoisomerase II (topo II), was used. Isolated nuclei were incubated in 50 μM dexrazoxane for half an hour in the cell incubator. For ATP experiments, isolated nuclei were incubated with 2 mg/mL ATP (A2383; Sigma-Aldrich) for 1 h at room temperature. An ATP depletion experiment was performed by incubating isolated nuclei in a depletion buffer containing 10 mM sodium azide (S2002; Sigma-Aldrich) and 50 mM 2-deoxyglucose (D8375; Sigma-Aldrich) for half an hour at room temperature. For OS experiments on mitotic HL60 chromosomes, cell synchronization was achieved by a standard double thymidine (Sigma-Aldrich) block and release protocol, and 10 μM dimethylenastron (VWR, Darmstadt, Germany) was applied for 10 h to keep the cells in the mitotic phase.

Quantifying nuclear volume and stiffness in the OS

The principle and setup of the microfluidic optical stretcher (OS) have been described extensively elsewhere (23,24). Cells or nuclei are made to flow through a microfluidic channel, before being serially trapped and/or heated by two diverging, counter-propagating Gaussian laser beams emanating from two optical fibers (see Fig. 2 A). Two OS setups are employed in this study, based on different wavelengths ($\lambda = 780$ or 1064 nm) operating on a single-mode, continuous-wave fiber laser. For the 1064 nm optical stretcher (YLM-5-1070-LP; IPG Photonics, Oxford, MA), the flow chamber was mounted on an inverted microscope (Axiovert 200M; Carl Zeiss, Oberkochen, Germany) equipped with a Plan Fluor ELWD 40×/NA 0.6 objective (Carl Zeiss), whereas for the 780 nm optical stretcher (Eylsa 780; Quantel, Les Ulis, France), the flow chamber was mounted on an inverted microscope (IX71; Olympus, Melville, NY) equipped with a Plan Fluor 40/NA 0.75 objective (Olympus). CCD cameras (Marlin F-146B; Allied Vision Technologies, Newburyport, MA) were attached to both setups for image acquisition. Channel flow was adjusted through the relative difference in heights of an inlet and outlet reservoir connected to the capillary. Representative deformation data were chosen from three or more independent experiments. The relative volume change was computed from the relative change of length along the major (b) and minor axes (a), assuming that suspended nuclei are prolate spheroids with volume $V = 4/3\pi a^2 b$. All volume changes were evaluated at $t = 1$ s after the step increase in temperature induced by laser. For minimal heating experiments performed with the 780 nm OS, nuclei were suspended in PBS prepared with heavy water (Sigma-Aldrich). For studies on changes in nuclear volume at different ambient temperatures, nuclei were seeded onto a heating chamber (BioCell; JPK Instruments, Berlin, Germany) that regulates temperature changes. Alternatively, nuclei were allowed to reach thermal equilibrium (20 min) in an OS where the stage temperature was controlled by the use of infrared lamp and heater, as adapted from previous study (25), before being optically trapped and having their volume measured. The trap power was minimal (0.2 W), corresponding to only ~0.4°C increase in temperature. Laser powers throughout are the sum of laser powers coming from the two opposing fibers.

To quantify the nuclear stiffness in minimal heating conditions (780 nm, heavy water), the optically induced stress was first computed using the

generalized Lorenz-Mie model (26). This requires a precise knowledge of the nuclear radii (determined in OS measurement), and their refractive index, which we previously determined using digital holographic microscopy (21). Once the peak stress σ_o along the laser axis was evaluated, the time-dependent creep compliance $J(t)$ could be readily obtained as

$$J(t) = \frac{\gamma(t)}{\sigma_o F_G}, \quad (1)$$

where the geometric factor F_G takes into account the nuclear size and stress distribution (27).

To extract cell viscoelastic parameters, we employed a power law model (28,29),

$$J(t) = J_o\left(\frac{t}{\tau_o}\right)^{\beta}. \quad (2)$$

Here, β is a measure of the effective nuclear fluidity, where $\beta = 0$ corresponds to the nuclei behaving like a perfectly elastic material, and $\beta = 1$ corresponds to the nuclei behaving like a purely viscous fluid; and J_o characterizes the compliance of the material, while the time is normalized by a timescale τ_o, which is set to 1 s. Because the nuclei were deformed in the linear regime in minimal heating experiments, we can convert the creep compliance to the complex modulus $G^*(f)$ using a Laplace transform (30). The storage modulus or the shear modulus is then given by $G'(f) = (\cos(\beta\pi/2)/J_o\Gamma(1+\beta))(2\pi f)^{\beta} = G_0(J_o,\beta)f^{\beta}$, where Γ is the gamma function. The prefactor G_0 (Shear modulus) can be easily calculated from the parameters J_o and β of our measured creep compliance, by taking $f = 1$ Hz.

Atomic force microscopy

Atomic force microscopy (AFM) indentation measurements were carried out with a CellHesion 200 (JPK Instruments) mounted on an Axiovert 200M inverted microscope (Carl Zeiss, Oberkochen, Germany) with 20×/NA 0.6 objective. A monodisperse polystyrene bead (10 μm in diameter) was glued onto a tipless silicon cantilever (Arrow TL1-50, spring constant: ~0.015 Nm^{-1}, confirmed by thermal fluctuation method; NanoWorld, Neuchâtel, Switzerland). Isolated nuclei swollen to various degrees in various concentrations of PBS were seeded onto poly-lysine-coated glass petri dishes for 10 min. All experiments were performed at room temperature. The nuclei were indented with a constant approach speed of 1 μm/s with a loading force of 1.5 nN. For each force-indentation curve, the apparent Young's modulus was determined by fitting the approach curve with the Hertz model for a spherical indentor, using the built-in JPK Instruments software. The fit was extended to an indentation depth of <10% of the nuclear height to minimize substrate stiffness effect (31). Nuclear sphericity was checked and confirmed by three-dimensional volume analysis (21). To correct for the different nuclear sizes, the effective radius of the tip curvature of the spherical indentor was obtained by using $(1/R_{\text{eff}}) = (1/R_{\text{nuclei}}) + (1/R_{\text{bead}})$. The Poisson ratio of the nuclei was taken to be 0.5. To minimize systematic errors, experiments were performed on nuclei prepared with different PBS conditions using the same calibrated cantilever on the same day. The average number of nuclei measured per experiment was ~60. Two or more independent experiments were performed for each condition at different dates to ensure reproducibility of results.

Fluorescence imaging of subnuclear structures

To image chromatin distribution, HL60 cells were incubated with Hoechst 33342 dye (Molecular Probes, Eugene, OR) with a final concentration of 5 μg/mL for 20 min before isolation. To stain for nuclear membrane, FM4-64 (Invitrogen, Carlsbad, CA) was added to the isolated nuclei with a final concentration of 100 ng/mL, and incubated for 10 min. Nuclei were then seeded onto poly-lysine-coated coverslips for 10 min before washing. To image nucleoli, cells were stained with NUCLEOLAR-ID Green Detection Reagent (1:1000; Enzo Life Sciences, Farmingdale, NY) according to manufacturer's instruction, before nuclear isolation. Samples were incubated for half an hour with primary antibodies recognizing nuclear pore complex (Mab414, dilution 1:500; Abcam, Cambridge, UK), lamin A/C (SAB4200236, 1:500; Sigma-Aldrich), HP1α (05-689, 1:500; Millipore), coilin (C1862, 1:500; Sigma-Aldrich), PML (HPA008312, 1:500; Sigma-Aldrich), or RNA pol II (SC-899, 1:500; Santa Cruz Biotechnology, Dallas, TX). The samples were then incubated at 4°C overnight. After washing, samples were incubated for 1 h with an appropriate secondary antibody conjugated with Alexa 488 (1:400; Molecular Probes), and washed again. All stained nuclei were imaged with an LSM700 inverted confocal microscope (40×, NA = 1.1, water immersion; Carl Zeiss). Gain settings were kept the same for all samples of a given experiment.

Image and fractal analysis

All statistical analysis was performed using the software Origin (Ver. 8.5; OriginLab, Northampton, MA). All box plots include whiskers at 5–95% range, horizontal box lines as SD, median line, and the mean (*inset box*). To quantify cortical thickness of chromatin at the nuclear periphery, a custom-written MATLAB code (The MathWorks, Natick, MA) based on a modification of Wertheimer's work (32) was used. The algorithm first converted the images into gray scale. After iterations of each ring from the boundary to the nuclear interior, the average fluorescence intensity of each ring was evaluated. Cortical thickness was determined when the average intensity of the ring dropped below the average intensity of the entire nucleus. The thickness of each ring was one pixel (30 nm). The average cortical density was defined as the average integrated fluorescence intensity over the circumferential area enclosed by the cortical layer. More than 25 nuclei were analyzed for nuclei of a particular volume.

Fractal analysis was performed with the FracLac plug-in in the software ImageJ (National Institutes of Health, Bethesda, MD). Fractal dimension was determined using the differential box counting method (33). Nuclear lacunarity was similarly quantified using the FracLac plug-in. Partially saturated images were excluded from the analysis.

RESULTS

pH, salts, and temperature alter nuclear volume in vitro

Before characterizing the material properties of isolated cell nuclei, we first checked the integrity of the nuclear architecture. Phase-contrast images of isolated HL60 nuclei trapped in an OS (Fig. 1 *A*) typically contain dark spots suggestive of the preservation of nucleoli, while Hoechst staining of DNA revealed heterogeneous distribution of chromatin structures within the nuclei. Previous studies have shown that some small, soluble proteins may leak out during the isolation procedure (34). We therefore examined by immunofluorescence staining the internal compartments of HL60 nuclei after chemical isolation in PBS buffer. As shown in Fig. 1 *A*, the nuclear membrane, nuclear pore complexes, lamin A/C, HP1α, nucleoli, PML bodies, Cajal bodies, and RNA polymerase II were all preserved, with characteristic morphology similar to those in intact cells. This is true even for nuclei under extreme swelling (Fig. S1). Our results suggest that the integrity and overall structure of the nuclei is not disturbed by the isolation procedure, in line with recent reports (20,21,35).

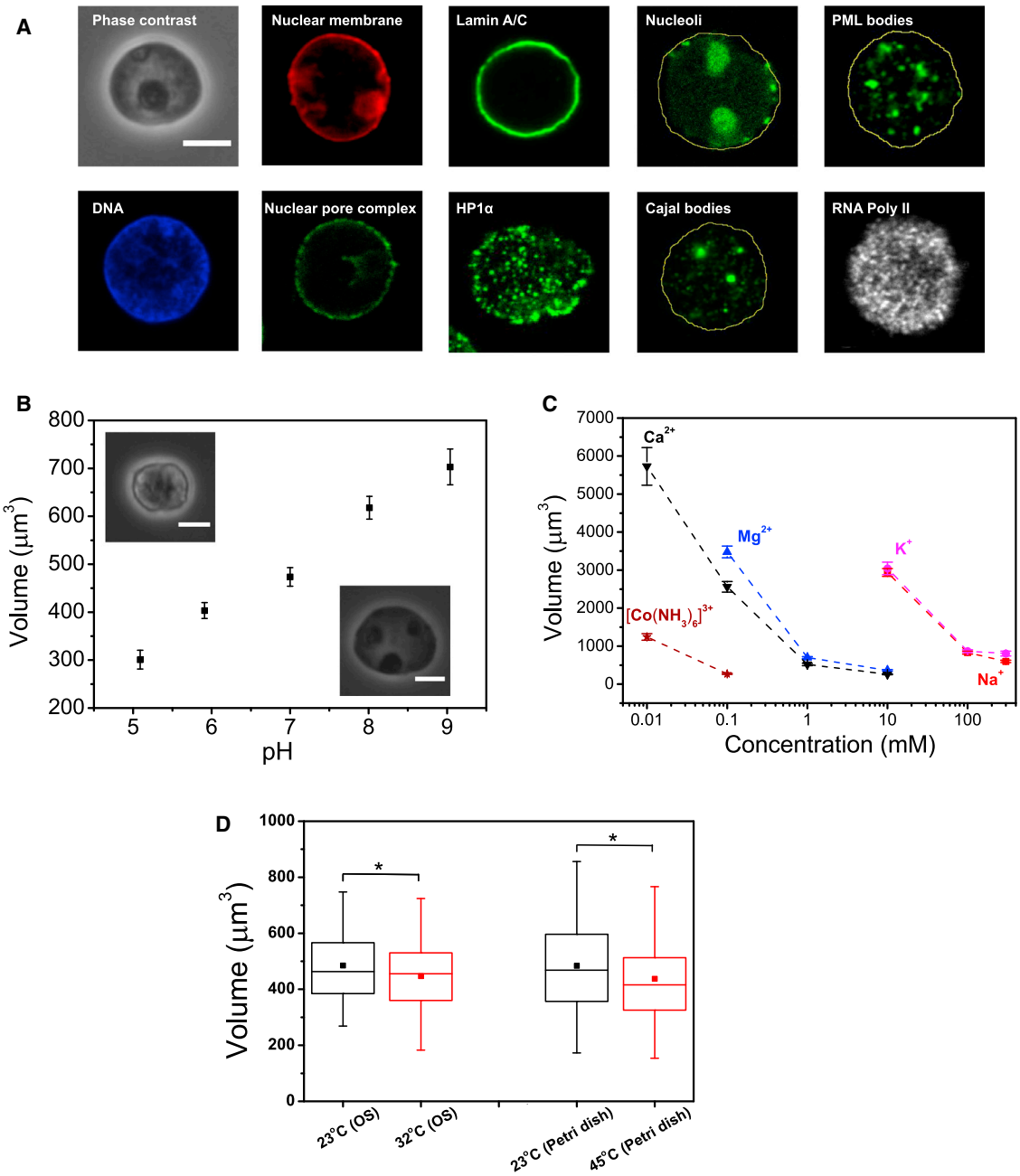

FIGURE 1 Nuclear volume is sensitive to changes in pH, salt conditions, and ambient temperature. (*A*) Nuclear compartmentalization is conserved after isolation. Immunofluorescence images (midsection confocal slices) of isolated HL60 nuclei stained for DNA (Hoechst), nuclear membrane (DID), nuclear pore complex (anti-nucleoporin), lamin A/C (anti-lamin A/C), HP1α (anti-HP1α), nucleoli (NUCLEOLAR-ID Green Detection Reagent), Cajal bodies (anti-coilin), PML bodies (anti-PML), and RNA polymerase II (anti-pol II). (*Yellow lines*) Approximate nuclear outlines. (*B*) Volume versus pH (mean $\pm$ SE) for optically trapped nuclei (trap power = 0.2 W, negligible heating). n = 26, 52, 47, 58, and 43 for pH = 5, 6, 7, 8, and 9, respectively. (*Insets*) Phase contrast images of nuclei at low and high pH. (*C*) Nuclear volume versus ionic concentrations of various valencies (mean $\pm$ SE). $n > 30$ for each salt condition. (*D*) Nuclear volume measured at different ambient temperatures in 780 nm OS (trap power = 0.2 W, n = 95 and 126 for 23°C and 32°C, respectively) and a heating Petri dish (n = 98, 83 for 23 and 45°C, respectively). $*p < 0.05$. Scale bars, 5 μm. To see this figure in color, go online.

Chromatin within cell nuclei is a highly compact structure made of histone proteins and DNA, which are negatively charged polyelectrolytes. It is known that counterions can screen the highly charged interior and maintain overall charge neutrality (36). To understand how the nuclear volume may be sensitive to the electrochemical conditions of the solvent, we quantified the volume of nuclei trapped in the OS at different pH solutions. As shown in Fig. 1 *B*, isolated HL60 nuclei swelled with increasing pH, from $V = 473 \pm 19$ μm^3 at pH = 7, to 618 ± 24 μm^3 (pH = 8)

and 703 ± 37 μm^3 (pH = 9). Swollen nuclei in alkaline pH appear to be optically homogeneous with a smooth nuclear membrane (see *inset*), whereas in acidic pH, the nuclei shrink ($V = 301 \pm 20$ μm^3 at pH = 5, and 403 ± 17 μm^3 at pH = 5.9) and appear granular, with uneven surface morphology. The lack of a pronounced sigmoidal shape of the transition across the large pH range indicates that nuclear swelling by pH shift is not a strongly cooperative phenomenon; that is, it is not equivalent to a phase transition.

Changes in the ionic conditions of the solvents may also influence nuclear volume. As shown in Fig. 1 *C*, in contrast to significant swelling at low concentrations of monovalent cations (~3000 μm^3 in 10 mM of NaCl or KCl buffer), the nuclei shrank to <900 μm^3 at higher concentrations (100 and 300 mM of NaCl or KCl buffer). The quantified nuclear volume was very similar in the two monovalent salts, despite the difference in their ionic radii. The volume change was more pronounced for nuclei in the presence of divalent cations, which occurred at much lower concentrations (<400 μm^3 in 10 mM of $MgCl_2$ or $CaCl_2$ buffer). In the presence of trivalent cations, such as Hexamminecobalt(III), nuclei can shrink to 270 ± 14 μm^3 with merely 0.1 mM. Similar to the nuclei in acidic condition, nuclei in dense multivalent salts displayed chromatin hypercondensation and uneven nuclear membrane.

We further studied whether nuclear volume is sensitive to changes in ambient temperatures, using a 780 nm OS housed within a heating chamber (see Materials and Methods) to quantify nuclear volume in their spherical state in suspension. We observed a slight volumetric reduction when the nuclei were preheated at 32°C, compared to those at 23°C (Fig. 1 *C*). Independent volume quantification for nuclei seeded onto Petri dishes heated to different temperatures further confirmed the slight reduction of nuclear volume at higher ambient temperatures. Overall, the changes to nuclear volume equilibrated at different ambient temperatures are smaller (if significant) compared to the volume changes associated with pH shifts or salt conditions.

Isolated nuclei increase their volume upon sudden increase of temperature

To investigate the influence of mechanical stress and transient heat on nuclear mechanics, two OS setups with different laser wavelengths (780 and 1064 nm) were employed to stretch cell nuclei in suspension (Fig. 2 *A*). The 780 nm OS was assembled from recently available 780 nm single-mode fiber lasers, which can deliver sufficiently high and stable laser power, with a minimal amount of laser-induced heat. The absorption coefficient of deionized water at 780 and 1064 nm is, respectively, 0.02 and 0.15 cm^{-1} (37). The absorption coefficient for heavy water is even lower than that of deionized water: at 780 nm, it is ~0.006 cm^{-1}. Previous studies using fluorescence ratio thermometry (25,38,39) showed that $\triangle T = 11°C\ W^{-1}$ in an 1064 nm OS, and that the temperature increase in the optical trap scales linearly with the absorption coefficient. Based on this finding, we therefore infer the temperature increase in the 780 nm OS to be $\triangle T = 1.5°C\ W^{-1}$ in deionized water and $\triangle T = 0.5°C\ W^{-1}$ in heavy water. Using PBS prepared with heavy water to further suppress heating, we characterized the mechanical properties of nuclei under optical stretching (Fig. 2 *B*). Nuclei in PBS prepared with heavy water, when stretched with a 780 nm OS, behaved as incompressible objects obeying volume conservation (Poisson ratio $\nu = 0.5$), as reflected in twice the amount of positive deformation along the major axis (*black*, *solid circles*) compared to the negative deformation along the minor axis (*black*, *open circles*). By fitting the data to the power law model and using the Laplace Transform (see Materials and Methods), we computed the Young's modulus of HL60 nuclei to be 538 ± 20 Pa, with a characteristic fluidity $\beta = 0.0923$ indicative of a solidlike nature.

Surprisingly, we find that this is not the case for nuclei in PBS prepared with deionized water, which incurred a slightly higher temperature increase (Fig. 2 *B*, *red*). In this case, the nuclei first responded normally upon stretch as characterized by the negative deformation along the minor axis, followed by gradual swelling along both the major and minor axes. The observed swelling of nuclei in response to only a few degrees increase in temperature is somewhat unexpected, and contrasts with cells or giant unilamellar vesicles under optical stretching (Fig. S2; Chan et al. (25)). Even more significant swelling was observed for nuclei stretched in the 1064 nm OS, which incurred greater amount of heating at the same laser power (Fig. 2 *C*). As expected, the use of heavy water dramatically reduced the swelling by almost 10-fold (*black*), compared to that prepared with deionized water (*red*). OS experiments on nuclei of other cell lines such as TNGA mouse embryonic stem cells and HeLa cells (Fig. S3) confirmed that such a swelling phenomenon, which we termed temperature-induced volume transition (TIVT), is not cell-specific. To investigate if heavy water modifies the intrinsic nuclear stiffness, which might account for the reduced TIVT, we performed AFM measurements at 23°C (Fig. S4). Our results showed that the nuclear stiffness in heavy water and deionized water are not significantly different, suggesting that the heavy water acts mainly to reduce the heat absorption in the nuclei. To introduce transient heat without inducing additional optical stress, we coupled a 1480 nm laser diode to one of the 1064 nm optical fibers, a technique we have previously established (25). The absorption coefficient at 1480 nm is ~180 times higher than that at 1064 nm, thereby imparting significant heating with only a few milliwatts. Using this approach, we found that TNGA nuclei in PBS swelled upon 1480 nm laser heating (Fig. S5), confirming that it is indeed the sudden temperature jump that triggers the nuclear volume increase.

We next investigated whether TIVT is reversible under repeated laser power increases (i.e., exhibits stretch).

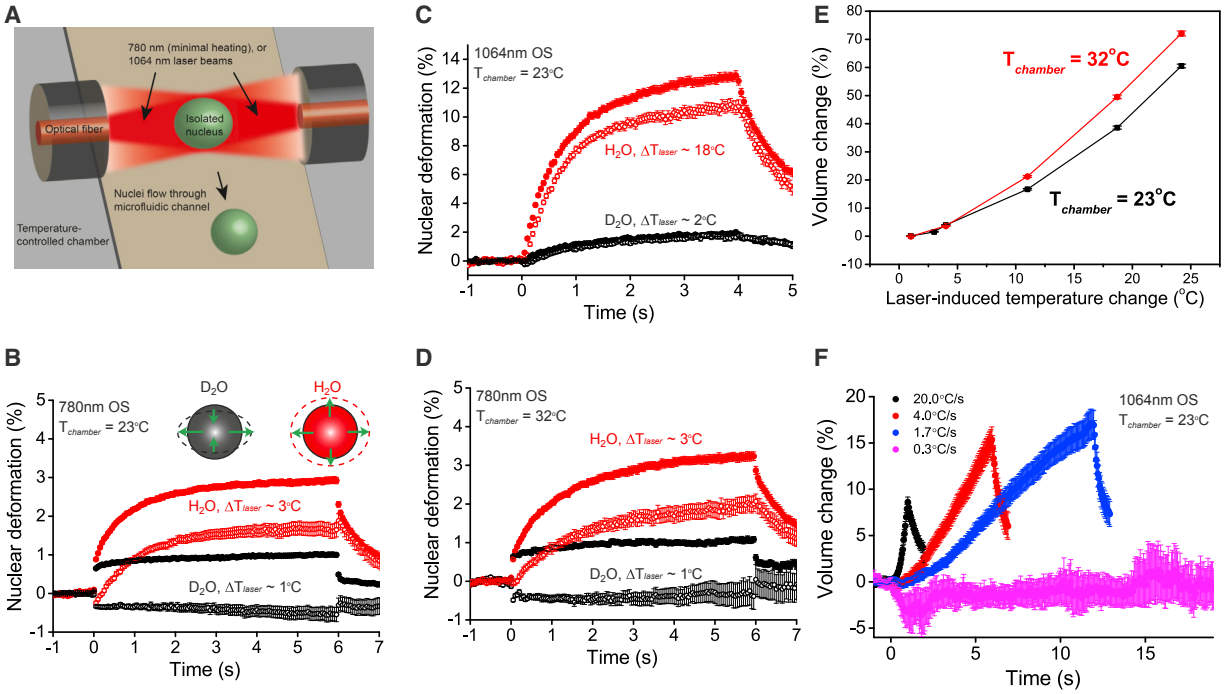

FIGURE 2 Temperature-induced volume transitions in isolated HL60 nuclei. (*A*) Schematic of OS operating with 1064 nm (significant heating) or 780 nm wavelength (reduced heating). Nuclei flowing through the microfluidic channel were serially trapped and stretched/heated by two counterpropagating laser beams. (*B*) Deformation curves for nuclei stretched in a 780 nm OS at 1.6 W at 23°C. In heavy water (*black*, $n = 104$), nuclei showed positive (and negative) deformation along the major (*solid circle*) and minor axes (*open circle*), respectively, indicating volume conservation. Replacing heavy water with deionized water led to an increase in temperature jump and swelling along both the major and minor axes (*red*, $n = 108$). (*C*) Deformation curves for nuclei stretched in a 1064 nm OS at 1.6 W at 23°C, in heavy (*black*, $n = 85$) and deionized water (*red*, $n = 53$). (*D*) Deformation curves for nuclei stretched in a 780 nm OS at 1.6 W at 32°C. Similar volume conservation in heavy water (*black*, $n = 53$) and swelling in deionized water (*red*, $n = 60$) were observed. (*E*) Temperature-induced volume change of nuclei at different ambient temperatures, based on collective data from both 780 and 1064 nm OS. $n > 40$ for each data point. (*F*) Volume changes for nuclei in response to linearly increasing laser powers in 1064 nm OS at 23°C. Maximum power reached was 2.2 W ($\Delta T_{\text{laser}} = 24$°C). Heat ramp was performed over 1 s (*black*, $n = 24$), 5 s (*red*, $n = 37$), 12 s (*blue*, $n = 22$), and 60 s (*magenta*, $n = 10$), with the respective rates of heat increase indicated in the legend. All error bars denote SE. To see this figure in color, go online.

Consecutive stretches were performed on individual nuclei, with ~10 s of rest time between each stretch. For isolated nuclei prepared with deionized water and heated in 780 nm OS, the deformation profiles for the first and second stretch overlapped with each other (Fig. S6), suggesting that the volume change is highly reversible with no visible hysteresis. In contrast, nuclei showed reduced TIVT during the second stretch in 1064 nm OS (Fig. S7), suggesting that strong heating could induce irreversible structural changes in nuclei and material hysteresis. We next investigated whether nuclear swelling occurred at a critical absolute temperature. Similar experiments were conducted in 780 nm OS at an elevated ambient temperature of 32°C (Fig. 2 *D*). We observed that similar to experiments conducted at 23°C, nuclei preheated at 32°C obeyed volume conservation in heavy water (*black*) but swelled in deionized water (*red*), when subjected to the same laser power increase. TIVT therefore does not occur at an absolute transition temperature, as is characteristic of volume phase transitions in equilibrium gel swelling (40). As shown in Fig. 2 *E*, nuclei preheated at 23 or 32°C exhibit nonlinear increase in swelling with increased heating. Interestingly, nuclei preheated at higher ambient temperature swelled more than those at room temperature, suggesting that prolonged heating may weaken the structural integrity of nuclei and their mechanical resistance against TIVT. To reconcile TIVT with the lack of swelling when nuclei were subjected to prolonged heating (Fig. 1 *D*), we applied a heat ramp, that is, a linearly increasing laser power at various rates of heating, to nuclei in the 1064 nm OS. As shown in Fig. 2 *F*, swelling occurs as long as the rate of heating remains above 1°C s^{-1}, which suggests that cell nuclei can remodel themselves to protect against volume change in the presence of slow adiabatic increase in ambient temperature. This could explain why nuclei did not swell under prolonged heating conditions in the OS or heated Petri dishes.

Temperature-induced volume transitions are sensitive to ionic conditions

Given that the equilibrium nuclear volume depends on the ionic conditions of the solvent (Fig. 1 *C*), we next studied whether TIVT exhibits a similar sensitivity to the ionic

conditions. We found that nuclei in monovalent salts experienced less temperature-induced volume increase with increasing concentrations, as was the case for 10 and 100 mM of KCl (Fig. 2 *A*). Notably, nuclei suspended in 0.1 mM $MgCl_2$ buffer displayed positive TIVT (swelling), but showed negative TIVT (contraction) in 1 mM $MgCl_2$ (Fig. 3 *B*; Movie S2). Upon heat application, an immediate contraction along both the major and minor axes was observed, followed by a slight rebound. The relaxation phase, after temperature was returned to baseline, shows a sudden jump to a higher deformation ($t = 4$ s), indicating that the heated nuclei were in a prestressed state. The deformation profile suggests two counteracting dynamics at play: an initial rapid contraction induced by multivalent charge effects, and a delayed swelling response. To investigate whether the nuclei contract in a heat-dependent manner, we performed similar OS experiments (780 nm OS) on nuclei suspended in 1 mM $CaCl_2$ prepared with heavy water (Fig. S8 *c*). In this minimal heating condition, nuclei still contracted along both axes, albeit with much less deformation, indicating that the strength of contraction correlates with the amount of temperature increase. Intriguingly, some nuclei in multivalent buffers rotated continuously around the major axis during the heating phase (Movie S3), and persisted until the laser power was turned off. The fraction of rotating nuclei was much higher in trivalent salts compared to divalent ones, and Ca^{2+} ions appeared to exert a greater impact on the rotational dynamics than Mg^{2+} ions (Fig. S9).

Fig. 3 *C* summarizes the distinct phases of TIVT under various ionic conditions. The upper, unshaded region depicts positive TIVT (swelling) while the lower, shaded region depicts negative TIVT (contraction). Nuclear contraction was measured as the peak contraction immediately after heat application. In the swelling regime, we find that nuclei in dilute divalent or trivalent salts, such as $CaCl_2$ (100 μM) and $Co(NH_3)_6Cl_3$ (10 μM), displayed reduced TIVT compared to those in high concentrations of NaCl or KCl (10 mM). A monotonous decrease in the magnitude of swelling was observed with increased ionic concentrations for both the monovalent and divalent cases, suggesting that increasing counterions contribute to greater mechanical resistance against TIVT. Increasing the concentrations of multivalent

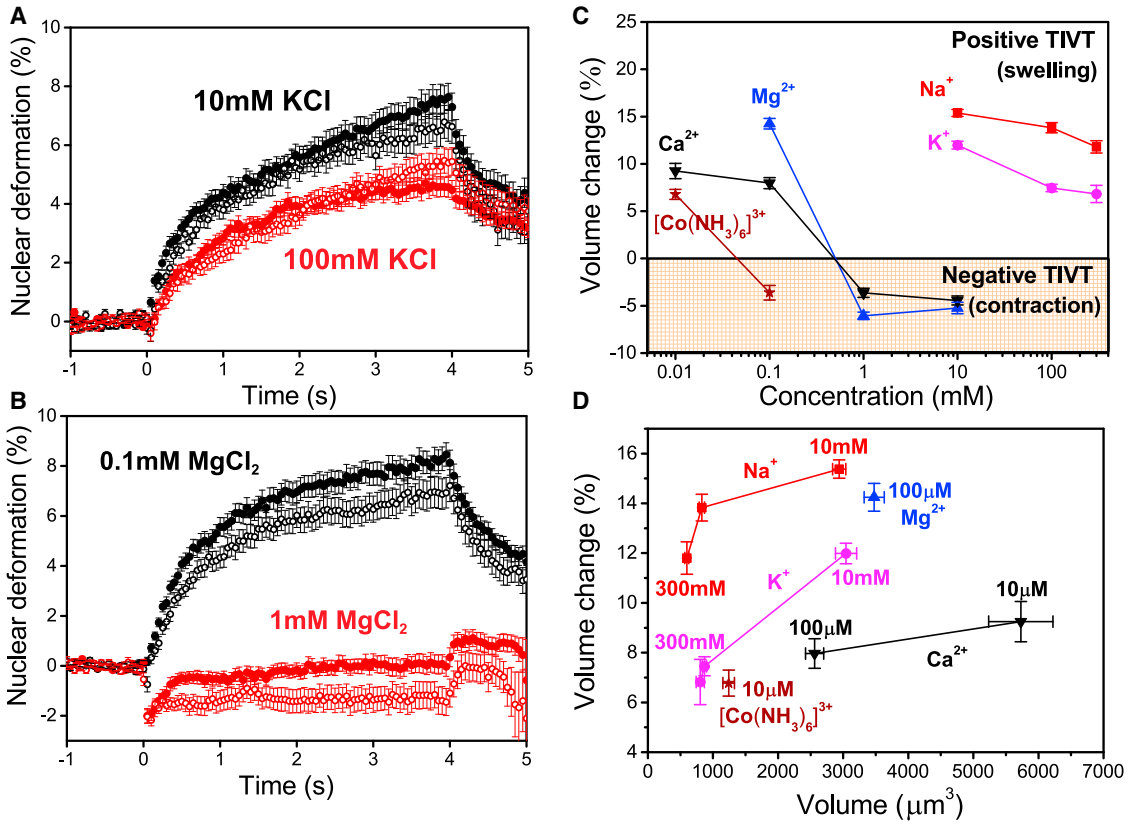

FIGURE 3 Temperature-induced volume transitions are sensitive to ionic conditions. (*A*) Deformation curves for HL60 nuclei in a 1064 nm OS at 23°C in 10 mM (*black*, $n = 30$), and 100 mM KCl (*red*, $n = 42$). (*B*) Deformation curves for HL60 nuclei in 0.1 mM (*black*, $n = 46$) and 1 mM $MgCl_2$ (*red*, $n = 52$). In both (*A*) and (*B*), the major deformation is denoted by the solid circles and the minor deformation by the open circles. (*C*) Phase diagram for TIVT in various salt conditions, depicting the transition to negative volume transitions in sufficiently high amounts of multivalent salts. (*D*) Volume changes of nuclei in salts of various valencies and concentrations as a function of initial nuclear volume. Temperature-induced swelling is sensitive to the valency and ionic radii of the salts. In all experiments, 1.7 W stretch power ($\Delta T_{laser} = 18°C$) was applied between $t = 0$ and 4 s. Volume changes were measured at $t = 1$ s into the stretch. $n > 30$ for each data point in (*C*) and (*D*). All error bars denote SE. To see this figure in color, go online.

ions led to a transition from swelling to contraction, with lower transition concentration observed for $Co(NH_3)_6^{3+}$. We further investigated whether a correlation existed between the degree of swelling and the initial nuclear size (Fig. 3 *D*). Despite their similar volume, nuclei in KCl displayed a smaller magnitude of TIVT than that of NaCl. The same trend was observed for nuclei in $CaCl_2$ compared to those in $MgCl_2$. This indicates that ionic radius is another factor influencing the amount of TIVT. Furthermore, Ca^{2+} ions impart greater stiffening of nuclei compared to the monovalent salts, even though the nuclei in Ca^{2+} salts are similar or larger in size than those in monovalent salts. For example, nuclei in 10 μM Ca^{2+} were much larger than those in 10 mM K^+ or Na^+ buffer, yet they displayed less swelling in response to heat. The same was observed for nuclei in 10 μM $Co(NH_3)_6^{3+}$ buffer, which were observed to be larger yet stiffer than those in 300 mM of Na^+ buffer. Overall, our findings identify multivalent salts as a critical determinant modulating the amount and sign of TIVT.

TIVTs are modulated by chromatin compaction

To investigate whether chromatin compaction state regulates TIVT, we diluted the chromatin by increasing the nuclear volume. Confocal images of Hoechst-stained nuclei swollen in various buffer (Fig. 4 *A*, *top row*) showed visible heterochromatin localized at the nuclear periphery and around the nucleoli. Such chromatin aggregation is not an artifact of isolation protocol because similar compartmentalization of chromatin was observed in situ (Fig. S10). In comparison to those in 20% and 5% PBS, nuclei in pure PBS displayed higher integrated fluorescence intensity with more condensed perinuclear heterochromatin. The average fluorescence intensity profile of a representative

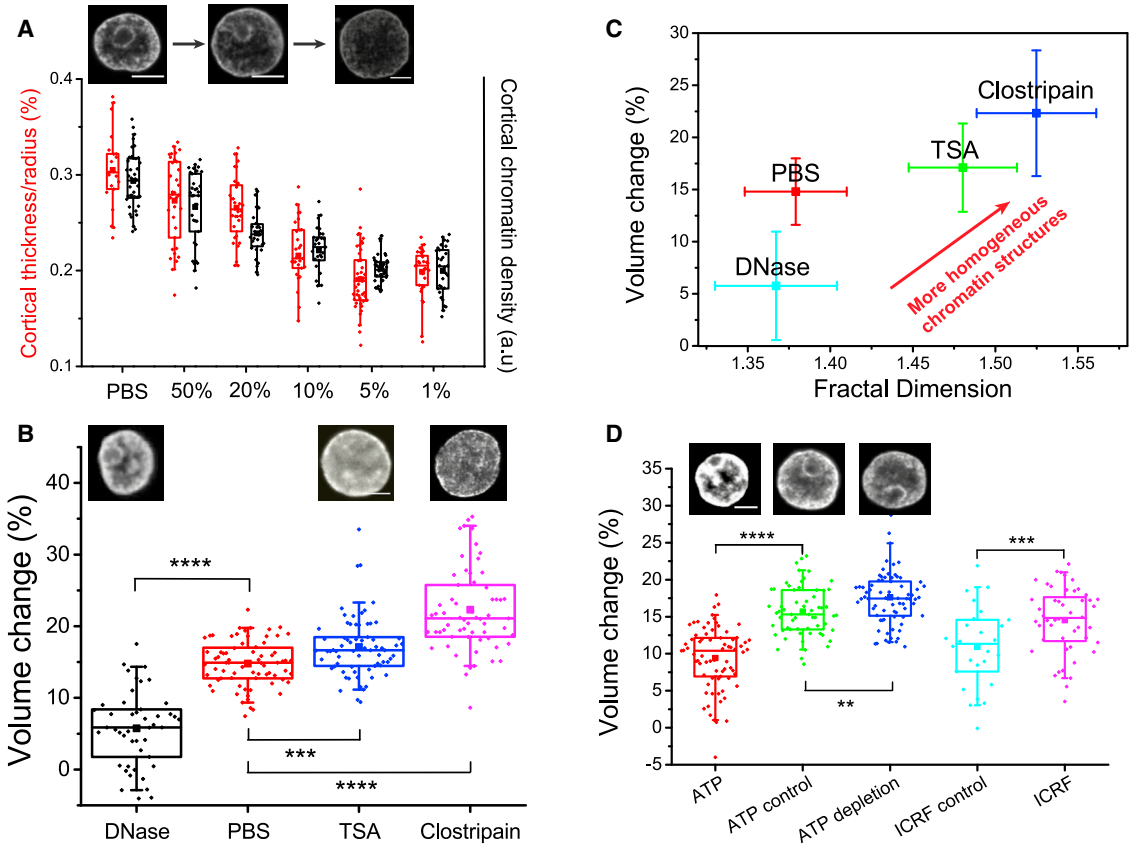

FIGURE 4 Temperature-induced volume transitions depend on chromatin compaction and remodeling dynamics. (*A*) Quantification of the relative thickness (*red*) and the average chromatin density (*black*) of the cortical chromatin shell for nuclei swollen to various degrees by PBS dilution. (*Top row*) DNA-stained nuclei in 100% PBS, 20% PBS, and 5% PBS. (*B*) Temperature-induced volume changes for nuclei under DNA degradation and histone modifications. (*Top row*) DNA-stained nuclei under corresponding pharmacological treatments. Nuclei treated with TSA ($n = 69$) and clostripain ($n = 63$) were significantly softer with larger TIVT than controls in PBS ($n = 72$). (*C*) Temperature-induced volume changes of nuclei versus fractal dimension. Addition of TSA ($n = 44$) and clostripain ($n = 27$) led to higher fractal dimension compared to control nuclei in PBS ($n = 21$) and DNase ($n = 17$). Error bars represent SD. (*D*). Temperature-induced volume changes of nuclei mediated by chromatin remodeling. Nuclei subjected to ATP addition ($n = 73$) or depletion ($n = 96$) showed less and more swelling effect, respectively, compared to the controls ($n = 61$). Topo II inhibition ($n = 48$) led to nuclear softening compared to the controls ($n = 26$). (*Top row*) DNA-stained nuclei under ATP addition or depletion, and in controls. All volume changes were measured at $t = 1$ s after optical stretching (laser powers = 1.7 W, $\Delta T_{laser} = 18°C$, 1064 nm). ****$p < 0.0001$, ***$p < 0.001$, and **$p < 0.01$. Scale bars represent 5 μm. To see this figure in color, go online.

nucleus in PBS (Fig. S11, *red curve*) shows a peak near the nuclear membrane followed by a gradual decrease toward the center of the nucleus, which allowed us to assign a shell thickness for the perinuclear heterochromatin (see Materials and Methods). We find that with PBS dilution, the cortical thickness did not vary much, leading to a net decrease in the ratio of cortical thickness to radius (Fig. 4 *A*, *red*). A similar drop in the average chromatin density associated with the heterochromatin shell was observed with swelling (Fig. 4 *A*, *black*), indicative of chromatin decondensation in the cortical layer. To investigate whether a thicker chromatin shell corresponds to a stiffer nucleus, we performed atomic force microscopy to characterize the elastic moduli of isolated nuclei (Fig. S12). Our results showed that the apparent nuclear stiffness scaled inversely with the nuclear volume.

Chromatin compaction can potentially influence the magnitude of TIVT. To this end, we modified chromatin compaction by pharmacological treatments and studied TIVT in several conditions (Fig. 4 *B*): TSA, a histone deacetylase inhibitor that decondenses chromatin (22); clostripain, a protease that decompacts chromatin by enzymatic cleavage of histone tails (8); and DNase I, a nuclease that cleaves DNA leading to DNA fragmentation. Nuclei treated with TSA exhibited highly homogeneous chromatin distribution throughout the entire nuclei with no visible heterochromatin at the nuclear periphery (*inset*). The volume change (17.10 $\pm$ 0.51%) for TSA-treated nuclei upon TIVT was significantly larger than that of the control nuclei in PBS (14.80 $\pm$ 0.38%). Clostripain-treated nuclei, with their highly fragmented chromatin, displayed even greater volume increase (22.32 $\pm$ 0.76%) upon TIVT. The volume increase was dramatically reduced for nuclei treated with DNase (5.76 $\pm$ 0.77%). Observation of DNA leakage out of the nuclei confirmed the drug effectiveness, although distinct regions of condensed chromatin could still be found within the nuclei.

To assess the chromatin compaction state, we quantified the fractal dimension of the chromatin distributions in confocal fluorescence images. Fractal dimension measures an object's uniformity: the more uniformly distributed the elements of the material, the higher the fractal dimension (10,41). Employing the differential box counting methodology (see Materials and Methods), we found that TSA and clostripain treatments led to an increase in fractal dimension and chromatin decondensation (Fig. 4 *C*). Additionally, we quantified the lacunarity of the nuclei (Fig. S13), which measures the distribution of voids in the nucleus (object heterogeneity instead of object uniformity) (42). TSA-treated nuclei had a lower lacunarity compared to the controls, indicating that chromatin decondensation led to a shrinkage of the pores and channels interdigitating the chromatin domains. Higher lacunarity was observed in nuclei in PBS and DNase, indicating uneven chromatin distribution punctuated by dark, chromatin-free pores. Both the fractal dimension and lacunarity analysis indicate that the more decondensed the chromatin structure, the larger the volume change incurred by TIVT, which can be taken as a proxy for nuclear stiffness.

Perturbation of chromatin remodeling processes, which has been shown to impact nuclear mechanics (43), may also affect the magnitude of TIVT. As shown in Fig. 4 *D*, ATP addition led to global compaction of chromatin (high fluorescence intensity) and a decrease in TIVT, while ATP depletion led to apparent chromatin decondensation and increased TIVT. We observed no significant difference in the initial volume between the control nuclei (5.50 $\pm$ 0.42 μm) and those with ATP addition (5.70 $\pm$ 0.64 μm) and depletion (5.86 $\pm$ 0.58 μm), suggesting that TIVT is modulated by ATP-dependent remodeling processes rather than changes in the initial nuclear volume. The remodeling processes are highly dynamic and reversible (Fig. S14). The pH of the buffer in all three conditions was the same, ruling out pH changes to the fluorescence emission characteristics of the Hoechst dye (44). Topo II, a major nuclear ATPase, can modify chromatin compaction by winding or unwinding the DNA loops, potentially modifying chromatin compaction and the magnitude of TIVT. We therefore studied the effect of ICRF-187, a known inhibitor of topo II, on TIVT. Interestingly, inhibiting topo II led to a significant increase in the magnitude of TIVT. Similar to ATP treatments, we found no significant difference in the initial nuclear volume between the controls (5.50 $\pm$ 0.51 μm) and the ICRF-187-treated nuclei (5.44 $\pm$ 0.36 μm).

DISCUSSION

Our work demonstrates that isolated nuclei can exhibit peculiar mechanical responses triggered by changes in their ambient temperature and modulated by the electrochemical environment. At constant temperature, the equilibrium volume depends on the pH or salt conditions (Fig. 1, *B* and *C*). As shown in previous osmotic studies of isolated chondrocyte nuclei (45), the nuclear envelope, punctuated with nuclear pore complexes, is highly permeable to small ions but not to the highly concentrated polyelectrolytes like chromatin. This sets up a high osmotic pressure within the nucleus, modulation of which can lead to significant volume change. As shown in our recent refractive index studies of isolated HL60 nuclei, hypertonic treatment (35 kDa PEG, 450 mOsm/kg) led to nuclear shrinkage while hypotonic treatment induced significant swelling (21). The chromatin assembly is stabilized by an attractive force mediated by histone tail-tail interactions, which counteract the repulsive electrostatic force between the negatively charged DNA segments (36,46). They are in turn bathed within a sea of positively charged screening counterions. According to the Flory-Rehner theory (47), the change in the free energy can be expressed as $\Delta F = \Delta F_{\mathrm{mix}} + \Delta F_{\mathrm{el}} + \Delta F_{\mathrm{ion}}$, where ΔF_{mix} is the mixing free energy, ΔF_{el} is the elastic contribution,

and ΔF_{ion} is the contribution from the electrostatic effects (counterion entropy). From these, the osmotic pressure can be split into three contributions: $\Pi = \Pi_{mix} + \Pi_{el} + \Pi_{ion}$, where $\Pi_{ion} = k_B T \sum_i (n_i^{in} - n_i^{out})$. Here n_i^{in} and n_i^{out} are the concentrations of species i in the gel and the surrounding solution, respectively. Equating chemical equilibrium and charge neutrality condition for the mobile ions inside and outside the nucleus, we have $\Pi_{ion} = k_B T n_b^2/4n_s$ (48,49), where n_b is the density of fixed ions in the nucleus. Decreasing salt concentrations n_s therefore leads to increased Π_{ion} and nuclear swelling, as shown in Fig. 1 *C*. Diluting the salts also reduces the amount of screening counterions in the nucleus, leading to increased net electrostatic repulsion between DNA segments and possibly structural expansion (though less significant than that generated by the osmotic pressure of mobile ions). With high concentrations of multivalent ions, counterion condensation can even induce charge reversal and attractive forces between the DNA, further compacting the nucleus (18,50) up to a hard core limit of chromatin, which is roughly 50% of the nuclear volume under isotonic conditions (51). In alkaline conditions, the H^+ in the nucleus combines with OH^- to form H_2O. To compensate for the net decrease in positive charges within the nucleus, deprotonation leads to a massive influx of salt cations, which can generate a large osmotic pressure and nuclear swelling at high pH (Fig. 1 *B*). Alternatively, deprotonation could lead to increased DNA-DNA electrostatic repulsion and chromatin expansion, similar to the swelling dynamics of RNA-filled viral capsids at high pH (52). However, this mechanism may be secondary to osmotic swelling in driving the significant swelling of nuclei at high pH.

At constant temperature, isolated nuclei behaved as highly elastic material with a stiffness of 538 ± 20 Pa, as determined by optical stretching. Previous studies using micropipette or microplates reported a stiffer Young's modulus (1–10 kPa) for isolated chondrocyte, epithelial, and endothelial cell nuclei (3,6,53), while AFM studies on isolated MCF10 nuclei revealed a similar range of stiffness (600 Pa) (54). Apart from a cell-specific issue such as the different levels of lamin A, which is a major contributor to nuclear mechanical properties, the differences in the measured stiffness may also be due to the different ionic/osmotic conditions, temperatures, and the magnitude/timescales of stress used in the various techniques. The overall strains employed in our OS and AFM studies (Fig. S12) are smaller (<5%) compared to other techniques, and they both measured similar values of nuclear stiffness. With minimal heating, we did not observe nuclear stiffening with repeated stretch (Fig. S6), in contrast to a recent report showing that isolated nuclei stiffen in response to repeated force application (55). This difference could be due to the local application of stress in their study, compared to our case in which we applied optical stress over the entire nuclear surface.

The central finding of the study is that isolated cell nuclei exhibit a volume transition in response to small, fast thermal perturbations. We termed it "temperature-induced volume transition" (TIVT) to distinguish it from the pH or salt-dependent volume changes at constant temperature. The immediate relaxation after TIVT, along with the overlap of the deformation curves with repeated temperature cycles (Fig. 2 *B*; Fig. S6), indicate that this phenomenon is transient and reversible. Interestingly, mitotic HL60 chromosomes devoid of nuclear lamina also displayed TIVT (Fig. S15). Collectively, these data provide evidence arguing against denaturation of nuclear lamina or nuclear pore complexes as the primary cause of TIVT. We ruled out swelling due to heat-induced pH changes in the solvent, because the pH of PBS decreases with increasing temperature, which would lead to nuclear shrinkage instead of swelling (Fig. 1 *B*). Thermal expansion of water is very unlikely because water has a volumetric coefficient of expansion of 0.02% K^{-1} at room temperature, which is negligible to account for TIVT (>3% volume expansion). Swelling due to thermophoresis, which could drive DNA flow along a temperature gradient (56), could not account for TIVT because previous OS studies based on fluorescence ratio thermometry (25,38) showed that for a small object such as a nucleus (diameter < 10 μm), heat is uniformly distributed throughout the nucleus without a temperature gradient. Altogether, our work identifies chromatin as the main structural component regulating volume changes in response to sudden temperature increase.

The observed swelling of nuclei induced by sudden heat application is reminiscent of the volume phase transition in thermoresponsive polyelectrolyte gels (40,57). Thermophilic hydrogels typically exhibit reversible swelling above an upper critical solution temperature (58). These transitions typically result from a competition between repulsive intermolecular forces acting to expand the polymer network, and an attractive force that acts to shrink it. In the nucleus, such forces could arise from electrostatic repulsion between the DNA segments and attractive histone tail-tail interactions. However, these are equilibrium phase transitions that occur at an absolute critical temperature, rather than at any ambient temperature as in our case (Fig. 2, *B* and *D*). Instead, we propose that the TIVT may be triggered by a sudden increase in the osmotic pressure Π_{ion} from the mobile ions within the nucleus. A small increase in thermal fluctuations may be sufficient to destabilize the counterions bound to the chromatin or the nonhistone proteins. The resultant increase in the free ion number density then generates strong Π_{ion}, which could cause the nuclear swelling. Importantly, TIVT depends on the rate of heating (Fig. 2 *F*). Rapid heating leads to reversible nuclear swelling, while with slow heating (<1°C s^{-1}), nuclei can remodel themselves adiabatically to maintain a constant volume. The slight nuclear contraction during prolonged heating (Fig. 1 *D*) could be attributed to changes in the lamina structure or protein denaturation in the nuclear matrix (13). Previous reports had shown that heating above 42°C causes invaginations of

perinuclear lamina (59), while osmotic change after cell detachment could lead to volumetric reduction of the nucleus and to envelope invagination (60). Invagination and weakening of lamina (61) could account for the observed nuclear softening and greater expansion at higher ambient temperatures (Fig. 2 *E*).

TIVT are also observed for nuclei in situ. OS experiments on whole cells showed that nuclei inside of cells may swell or contract, depending on the cell types (Fig. S16). The sign of TIVT could be influenced by the prevalent kind of cytoplasmic ions (mono versus multivalent) and their concentrations in the vicinity of the nucleus. In contrast to isolated nuclei, nuclei in situ still exhibit volume transitions with minimal heating (Fig. S16, *c* and *d*), which could be due to force transmission from the cell surface via the cytoskeleton to the nucleus. Alternatively, the heavy water outside the cell may not be able to permeate the cell cytoplasm and reach the nucleus, due to strong binding of structured water to charged fibrous gel in the cytoplasm. Using a laser to heat up gold nanoparticles in the nuclei of living neurons, Romero et al. (62) reported a correlation between nuclear expansion and the intensity of irradiation. Similarly, using a 1450 nm IR laser to heat individual adherent HeLa cells, one research group (M. Kreysing, personal communication) observed reversible swelling of chromatin compartments when heating by 4 to 10 Kelvin at a physiological ambient temperature of 37°C.

While situations where cells experience this kind of sudden temperature jump may be rare, our findings imply that TIVT could lead to massive influx of cytoplasmic fluid into the nucleoplasm, which could facilitate molecular turnover and transcriptional/mRNA activities. For example, the enzymatic activity of DNA repair enzymes, which act to preserve DNA damage, is highly dependent on the distribution and the amount of water accessible within the nucleus (via diffusion). Recent work indeed indicates that the nucleoplasm could be largely aqueous in facilitating such processes (21). Similarly, temperature-induced nuclear swelling could draw free cytosolic ions, which can potentially modify chromatin compaction state and facilitate or suppress transcriptional activities.

Ionic conditions not only determine the magnitude, but also the sign of TIVT (Fig. 3). As discussed before, increased concentrations of monovalent salts led to a smaller osmotic pressure Π_{ion} and nuclear volume (Fig. 1 *C*). This implies a greater free energy cost against external mechanical deformation (36), which may account for the increased resistance against TIVT (Fig. 3, *A* and *C*). Larger nuclei in strong ionic buffer (e.g., 10 μM Ca^{2+}) exhibited less volume increase than smaller nuclei in weak ionic buffer (e.g., 10 mM Na^{+}) (Fig. 3 *D*), suggesting that the ionic strength exerts a more significant impact on TIVT than the initial nuclear size. At high concentrations of multivalent salts, nuclei can display negative TIVT (Fig. 3, *B* and *C*). It is known that in multivalent salts, DNA condenses into a highly compact and ordered toroidal structure (18,63). Chromosome hypercondensation at millimolar concentrations of multivalent ions has also been reported by Poirier et al. (64), who showed that isolated mitotic chromosomes displayed rapid, reversible contraction and increased stiffness upon exposure to $MgCl_2$ or $CaCl_2$. Substantial volumetric reduction was also observed for chromosomes upon addition of $Co(NH_3)_6^{3+}$ buffer, in line with our studies (Fig. 3 *D*). Such compaction is known to arise from strongly correlated counterion-induced attraction between DNA segments, otherwise known as "Manning condensation" or "charge inversion" (50,65,66). Our results therefore suggest that a sudden temperature jump may trigger an influx of multivalent ions, leading to multivalent-ion-induced DNA condensation and global chromatin hypercompaction. The occasional nuclear rotations in multivalent salts suggest that chromatin condensation could induce the formation of orientationally ordered microdomains or helical structures in nuclear lamina, giving rise to bulk birefringence. Conservation of angular momentum of the linearly polarized laser light could then lead to the observed nuclear rotations. Future work will be required to shed light on the detailed mechanism underlying this process. Finally, we note that nuclei under hypertonic shock, despite having similar compactness and surface invagination as those in multivalent ions (e.g., 1 mM Ca^{2+}), exhibit positive TIVT and no rotations (Fig. S17). This further affirms that the negative TIVT in strong multivalent salts arises primarily from strong charge effects.

Confocal imaging (Fig. 4 *A*; Fig. S1) revealed that in HL60 cell nuclei, chromatin preferentially localized to the perinuclear region. The decrease in the relative thickness of heterochromatin shell and its chromatin density after PBS dilution (Fig. 4 *A*) may be explained by the conformational change of chromatin fibers from an extended, unfolded 10 nm beads-on-a-string structure to condensed 30 nm fibers, as the NaCl concentration increases from 10 to 150 mM (36). The increased susceptibility to TIVT (taken as a proxy for nuclear softness) after chromatin dilution (Fig. 4, *B* and *C*; Fig. S12) agrees with recent AFM and micropattern studies (5,6,8). While we measured a considerably lower Young's moduli than those reported in these studies, possibly due to the different bead size, indentation rate, or forces used, we obtained a similar inverse correlation between nuclear volume and chromatin condensation.

Chromatin perturbation shows that modifying histone tail-tail interactions through histone acetylation (TSA) or proteolysis (clostripain) can significantly impact TIVT. TSA weakens the electrostatic interactions between the histone tails and the DNA backbone, leading to chromatin decondensation (22) and increased (decreased) fractal dimension (lacunarity) (Fig. 4 *C*; Fig. S13). The increased magnitude of TIVT (a proxy for nuclear softness) with TSA treatment (Fig. 4 *B*) corroborates recent nuclear mechanical studies (9,10). Clostripain, a protease that cleaves the residues of the amino acid arginine, leads to global decompaction of chromatin and nuclear volume increase,

possibly due to entropic swelling (8). This is consistent with their highly fragmented and homogeneous chromatin distribution, and high fractal dimension and low lacunarity (Fig. 4 *C*; Fig S13). Clostripain-treated nuclei were highly susceptible to TIVT, suggesting that the dissociation of heterochromatin nodes, which anchor to the nuclear lamin, is crucial in maintaining nuclear mechanical integrity. Notably, clostripain-treated nuclei, despite being smaller (7.41 $\pm$ 0.70 μm), deform much more than nuclei in 5% PBS (10.84 $\pm$ 0.97 μm), indicating that nuclear softening is caused mainly by the structural weakening of the tertiary chromatin architecture. Intriguingly, contrary to previous study (6), DNase-treated nuclei appeared smaller and stiffer than nuclei in PBS (Fig. 4 *B*). Our results, however, agree with other studies that reported substantial DNA leakage after DNase treatment (8,46).

The addition of ATP induced rapid, reversible chromatin compaction and nuclear stiffening, in contrast to chromatin decondensation and softening in ATP-depleted nuclei (Fig. 4 *D*). Hameed et al. (67) observed that ATP depletion or TSA led to a reduction of hopping movements of beads in the nucleus upon force application, which they attributed to the reduced free-volume in the nucleus. This is consistent with our observation of chromatin decondensation and a reduced lacunarity in both ATP-depleted and TSA treated nuclei. ATP also activates chromatin remodeling complexes and triggers nucleosome packing, thereby inducing global chromatin compaction (68), in line with our observation. Interestingly, ATP is required for chromatin condensation during early events of apoptosis (69), and ATP-depleted HL60 cells exhibit DNA fragmentation and chromatin decondensation (70). Inhibition of topo II activity led to nuclear softening, suggesting that topo II may contribute to nuclear stiffness. Topo II is known to localize to the nuclear matrix fraction of interphase nuclei and the scaffold fraction of the mitotic chromosome (71), and is responsible for the decatenation and relaxation of the DNA double strands through resolving DNA entanglements. Micropipette studies by Kawamura et al. (72) had shown that topo II reduces the elastic stiffness of mitotic chromosome while inhibition of topo II with ICRF-187 blocks this effect. Other studies, however, reported that topo II mediates DNA assembly and promotes chromatin compaction (73). Our results appeared to support the latter case, which could hint at potential differences in the structural maintenance role of topo II in interphase chromatin and mitotic chromosome.

In conclusion, we have demonstrated that isolated cell nuclei exhibit rich phases of temperature-induced volume transitions, depending on the electrochemical environment and chromatin compaction state. In contrast to nuclei at constant temperatures that behave as highly stiff and elastic material, whose volume is sensitive to pH and salt conditions, nuclei subjected to a sudden temperature increase displayed reversible and repeatable volume transitions. The sign and magnitude of TIVT can be modulated by the solvent ionic conditions and chromatin compaction, elucidating the roles of counterion exchange and heterochromatin integrity in governing nuclear hydration dynamics. Determination of the exact molecular mechanisms using concepts from polymer gel physics will be an exciting aspect for future nuclear mechanics research. While the physiological relevance of the phenomenon of rapid nuclear volume transitions are unclear at present, our findings may have implications for understanding nuclear volume regulation, and could be seen in line with other thermodynamic transitions occurring within the cells, such as phase separation of RNA-protein bodies or sol-gel phase transitions of the cytoplasm (74,75).

SUPPORTING MATERIAL

Seventeen figures and three movies are available at http://www.biophysj.org/biophysj/supplemental/S0006-3495(17)30143-1.

AUTHOR CONTRIBUTIONS

C.J.C. and J.G. designed the experiments; C.J.C. and W.L. performed all the experiments and analysis; G.C. helped with building the 780 nm optical stretcher; and C.J.C. wrote the article, with editorial assistance from all co-authors.

ACKNOWLEDGMENTS

The authors are grateful for insightful discussions with Don and Ada Olins, Helmut Schiessel, Dennis Discher, Elisabeth Fischer-Friedrich, Bela Mulder, Paul Janmey, Gijsje Koenderink, and Andreas Fery. The authors acknowledge Andrew Ekpenyong for preliminary work in assembling the 780 nm optical stretcher, Mirjam Schürmann for help with digital holographic microscopy, and the light microscopy facility of BIOTEC/CRTD.

The authors acknowledge financial support from the European Community's Seventh Framework Program (FP7/2007-2013) under grant agreement No. TRANSPOL-264399 (C.J.C. and J.G.), the "LightTouch" Starting Investigator Grant (No. 282060) of the European Research Council (J.G.), and a Humboldt-Professorship from the Alexander-von-Humboldt-Foundation (J.G.). The light microscopy facility of BIOTEC/CRTD is, in part, funded by the State of Saxony and the European Fund for Regional Development (EFRD).

REFERENCES

1. Lammerding, J., J. Hsiao, …, R. T. Lee. 2005. Abnormal nuclear shape and impaired mechanotransduction in emerin-deficient cells. *J. Cell Biol.* 170:781–791.
2. Swift, J., I. L. Ivanovska, …, D. E. Discher. 2013. Nuclear lamin-A scales with tissue stiffness and enhances matrix-directed differentiation. *Science.* 341:1240104.
3. Guilak, F., J. R. Tedrow, and R. Burgkart. 2000. Viscoelastic properties of the cell nucleus. *Biochem. Biophys. Res. Commun.* 269:781–786.
4. Maniotis, A. J., C. S. Chen, and D. E. Ingber. 1997. Demonstration of mechanical connections between integrins, cytoskeletal filaments, and nucleoplasm that stabilize nuclear structure. *Proc. Natl. Acad. Sci. USA.* 94:849–854.
5. Versaevel, M., T. Grevesse, and S. Gabriele. 2012. Spatial coordination between cell and nuclear shape within micropatterned endothelial cells. *Nat. Commun.* 3:671.

6. Dahl, K. N., A. J. Engler, …, D. E. Discher. 2005. Power-law rheology of isolated nuclei with deformation mapping of nuclear substructures. *Biophys. J.* 89:2855–2864.
7. Pajerowski, J. D., K. N. Dahl, …, D. E. Discher. 2007. Physical plasticity of the nucleus in stem cell differentiation. *Proc. Natl. Acad. Sci. USA.* 104:15619–15624.
8. Mazumder, A., T. Roopa, …, G. V. Shivashankar. 2008. Dynamics of chromatin decondensation reveals the structural integrity of a mechanically prestressed nucleus. *Biophys. J.* 95:3028–3035.
9. Krause, M., J. Te Riet, and K. Wolf. 2013. Probing the compressibility of tumor cell nuclei by combined atomic force-confocal microscopy. *Phys. Biol.* 10:065002.
10. Chalut, K. J., M. Höpfler, …, J. Guck. 2012. Chromatin decondensation and nuclear softening accompany Nanog downregulation in embryonic stem cells. *Biophys. J.* 103:2060–2070.
11. Pagliara, S., K. Franze, …, K. J. Chalut. 2014. Auxetic nuclei in embryonic stem cells exiting pluripotency. *Nat. Mater.* 13:638–644.
12. Meyer, S., D. Jost, …, R. Everaers. 2013. Temperature dependence of the DNA double helix at the nanoscale: structure, elasticity, and fluctuations. *Biophys. J.* 105:1904–1914.
13. Lepock, J. R. 2005. How do cells respond to their thermal environment? *Int. J. Hyperthermia.* 21:681–687.
14. Lepock, J. R., H. E. Frey, …, R. L. Warters. 2001. The nuclear matrix is a thermolabile cellular structure. *Cell Stress Chaperones.* 6:136–147.
15. Warmt, E., T. R. Kießling, …, J. Käs. 2014. Thermal instability of cell nuclei. *New J. Phys.* 16:073009.
16. Fudenberg, G., and L. A. Mirny. 2012. Higher-order chromatin structure: bridging physics and biology. *Curr. Opin. Genet. Dev.* 22:115–124.
17. Emanuel, M., N. H. Radja, …, H. Schiessel. 2009. The physics behind the larger scale organization of DNA in eukaryotes. *Phys. Biol.* 6:025008.
18. Bloomfield, V. A. 1997. DNA condensation by multivalent cations. *Biopolymers.* 44:269–282.
19. Thoumine, O., A. Ott, …, J. J. Meister. 1999. Microplates: a new tool for manipulation and mechanical perturbation of individual cells. *J. Biochem. Biophys. Methods.* 39:47–62.
20. Suzuki, K., P. Bose, …, K. Riabowol. 2010. REAP: a two minute cell fractionation method. *BMC Res. Notes.* 3:294.
21. Schürmann, M., J. Scholze, …, C. J. Chan. 2016. Cell nuclei have lower refractive index and mass density than cytoplasm. *J. Biophotonics.* 9:1068–1076.
22. Tóth, K. F., T. A. Knoch, …, K. Rippe. 2004. Trichostatin A-induced histone acetylation causes decondensation of interphase chromatin. *J. Cell Sci.* 117:4277–4287.
23. Guck, J., R. Ananthakrishnan, …, J. Käs. 2001. The optical stretcher: a novel laser tool to micromanipulate cells. *Biophys. J.* 81:767–784.
24. Lincoln, B., F. Wottawah, …, J. Guck. 2007. High-throughput rheological measurements with an optical stretcher. *Methods Cell Biol.* 83:397–423.
25. Chan, C. J., G. Whyte, …, J. Guck. 2014. Impact of heating on passive and active biomechanics of suspended cells. *Interface Focus.* 4:20130069.
26. Boyde, L., A. Ekpenyong, …, J. Guck. 2012. Comparison of stresses on homogeneous spheroids in the optical stretcher computed with geometrical optics and generalized Lorenz-Mie theory. *Appl. Opt.* 51:7934–7944.
27. Ananthakrishnan, R., J. Guck, …, J. Käs. 2006. Quantifying the contribution of actin networks to the elastic strength of fibroblasts. *J. Theor. Biol.* 242:502–516.
28. Maloney, J. M., E. Lehnhardt, …, K. J. van Vliet. 2013. Mechanical fluidity of fully suspended biological cells. *Biophys. J.* 105:1767–1777.
29. Chan, C. J., A. E. Ekpenyong, …, F. Lautenschläger. 2015. Myosin II activity softens cells in suspension. *Biophys. J.* 108:1856–1869.
30. Desprat, N., A. Richert, …, A. Asnacios. 2005. Creep function of a single living cell. *Biophys. J.* 88:2224–2233.
31. Fischer-Cripps, A. C. 2000. A review of analysis methods for submicron indentation testing. *Vacuum.* 58:569–585.
32. MacQueen, L. A., M. Thibault, …, M. R. Wertheimer. 2012. Electromechanical deformation of mammalian cells in suspension depends on their cortical actin thicknesses. *J. Biomech.* 45:2797–2803.
33. Lopes, R., and N. Betrouni. 2009. Fractal and multifractal analysis: a review. *Med. Image Anal.* 13:634–649.
34. Paine, P. L., C. F. Austerberry, …, S. B. Horowitz. 1983. Protein loss during nuclear isolation. *J. Cell Biol.* 97:1240–1242.
35. Hancock, R., and Y. Hadj-Sahraoui. 2009. Isolation of cell nuclei using inert macromolecules to mimic the crowded cytoplasm. *PLoS One.* 4:e7560.
36. Korolev, N., A. Allahverdi, …, L. Nordenski. 2012. The polyelectrolyte properties of chromatin. *Soft Matter.* 8:9322–9333.
37. Kedenburg, S., M. Vieweg, …, H. Giessen. 2012. Linear refractive index and absorption measurements of nonlinear optical liquids in the visible and near-infrared spectral region. *Opt. Mater. Express.* 2:1588.
38. Ebert, S., K. Travis, …, J. Guck. 2007. Fluorescence ratio thermometry in a microfluidic dual-beam laser trap. *Opt. Express.* 15:15493–15499.
39. Delabre, U., K. Feld, …, J. Guck. 2015. Deformation of phospholipid vesicles in an optical stretcher. *Soft Matter.* 11:6075–6088.
40. Annaka, M., and T. Tanaka. 1992. Multiple phases of polymer gels. *Nature.* 355:430–432.
41. Recamier, V., I. Izeddin, …, X. Darzacq. 2014. Single cell correlation fractal dimension of chromatin A framework to interpret 3D single molecule. *Nucleus.* 5:75–84.
42. Chalut, K. J., K. Kulangara, …, K. W. Leong. 2011. Stem cell differentiation indicated by noninvasive photonic characterization and fractal analysis of subcellular architecture. *Integr. Biol.* 3:863–867.
43. Shivashankar, G. V. 2011. Mechanosignaling to the cell nucleus and gene regulation. *Annu. Rev. Biophys.* 40:361–378.
44. Barooah, N., J. Mohanty, …, A. C. Bhasikuttan. 2011. pH and temperature dependent relaxation dynamics of Hoechst-33258: a time resolved fluorescence study. *Photochem. Photobiol. Sci.* 10:35–41.
45. Finan, J. D., K. J. Chalut, …, F. Guilak. 2009. Nonlinear osmotic properties of the cell nucleus. *Ann. Biomed. Eng.* 37:477–491.
46. Mazumder, A., T. Roopa, …, G. V. Shivashankar. 2010. Prestressed nuclear organization in living cells. *Methods Cell Biol.* 98:221–239.
47. Flory, P. J., and J. Rehner. 1943. Statistical mechanics of cross-linked polymer networks II. Swelling. *J. Chem. Phys.* 11:521–526.
48. Doi, M. 2013. Soft Matter Physics. Oxford University Press, Oxford, UK.
49. Quesada-Pérez, M., J. A. Maroto-Centeno, …, R. Hidalgo-Alvarez. 2011. Gel swelling theories: the classical formalism and recent approaches. *Soft Matter.* 7:10536.
50. Besteman, K., K. van Eijk, and S. G. Lemay. 2007. Charge inversion accompanies DNA condensation by multivalent ions. *Nat. Phys.* 3:641–644.
51. Irianto, J., C. R. Pfeifer, …, D. E. Discher. 2016. Nuclear constriction segregates mobile nuclear proteins away from chromatin. *Mol. Biol. Cell.* 27:4011–4020.
52. Wilts, B. D., I. A. T. Schaap, and C. F. Schmidt. 2015. Swelling and softening of the cowpea chlorotic mottle virus in response to pH shifts. *Biophys. J.* 108:2541–2549.
53. Caille, N., O. Thoumine, …, J.-J. Meister. 2002. Contribution of the nucleus to the mechanical properties of endothelial cells. *J. Biomech.* 35:177–187.
54. Li, Q., and C. Lim. 2010. Structure-mechanical property changes in nucleus arising from breast cancer. *In* Cellular and Biomolecular Mechanics and Mechanobiology. Springer, Berlin, Germany, pp. 465–475.
55. Guilluy, C., L. D. Osborne, …, K. Burridge. 2014. Isolated nuclei adapt to force and reveal a mechanotransduction pathway in the nucleus. *Nat. Cell Biol.* 16:376–381.

56. Duhr, S., and D. Braun. 2006. Why molecules move along a temperature gradient. *Proc. Natl. Acad. Sci. USA.* 103:19678–19682.

57. Mah, E., and R. Ghosh. 2013. Thermo-responsive hydrogels for stimuli-responsive membranes. *Processes.* 1:238–262.

58. Ilmain, F., T. Tanaka, and E. Kokufuta. 1991. Volume transition in a gel driven by hydrogel bonding. *Nature.* 349:400–401.

59. Falloon, E. A., and J. R. Dynlacht. 2002. Reversible changes in the nuclear lamina induced by hyperthermia. *J. Cell. Biochem.* 86:451–460.

60. Kim, D.-H., B. Li, …, S. X. Sun. 2015. Volume regulation and shape bifurcation in the cell nucleus. *J. Cell Sci.* 128:3375–3385.

61. Geggier, S., A. Kotlyar, and A. Vologodskii. 2011. Temperature dependence of DNA persistence length. *Nucleic Acids Res.* 39:1419–1426.

62. Romero, V. H., Z. Kereselidze, …, X. G. Peralta. 2014. Nanoparticle assisted photothermal deformation of individual neuronal organelles and cells. *Biomed. Opt. Express.* 5:4002–4012.

63. Conwell, C. C., and N. V. Hud. 2004. Evidence that both kinetic and thermodynamic factors govern DNA toroid dimensions: effects of magnesium(II) on DNA condensation by hexammine cobalt(III). *Biochemistry.* 43:5380–5387.

64. Poirier, M. G., T. Monhait, and J. F. Marko. 2002. Reversible hypercondensation and decondensation of mitotic chromosomes studied using combined chemical-micromechanical techniques. *J. Cell. Biochem.* 85:422–434.

65. Ray, J., and G. S. Manning. 1994. An attractive force between two rodlike polyions mediated by the sharing of condensed counterions. *Langmuir.* 10:2450–2461.

66. Schiessel, H., and P. Pincus. 1998. Counterion-condensation-induced collapse of highly charged polyelectrolytes. *Macromolecules.* 31:7953–7959.

67. Hameed, F. M., M. Rao, and G. V. Shivashankar. 2012. Dynamics of passive and active particles in the cell nucleus. *PLoS One.* 7:e45843.

68. Alberts, B., A. Johnson, …, P. Walter. 2002. Molecular Biology of the Cell, Ed. 4. Garland Science, New York.

69. Kass, G. E. N., J. E. Eriksson, …, S. C. Chow. 1996. Chromatin condensation during apoptosis requires ATP. *Biochem. J.* 318:749–752.

70. Nakamura, N., and Y. Wada. 2000. Properties of DNA fragmentation activity generated by ATP depletion. *Cell Death Differ.* 7:477–484.

71. Marko, J. F. 2011. The mitotic chromosome: structure and mechanics. *In* Genome Organization and Function in the Cell Nucleus, 1st Ed. John Wiley, Hoboken, NJ.

72. Kawamura, R., L. H. Pope, …, J. F. Marko. 2010. Mitotic chromosomes are constrained by topoisomerase II-sensitive DNA entanglements. *J. Cell Biol.* 188:653–663.

73. Hizume, K., S. Araki, …, K. Takeyasu. 2007. Topoisomerase II, scaffold component, promotes chromatin compaction in vitro in a linker-histone H1-dependent manner. *Nucleic Acids Res.* 35:2787–2799.

74. Munder, M. C., D. Midtvedt, …, S. Alberti. 2016. A pH-driven transition of the cytoplasm from a fluid- to a solid-like state promotes entry into dormancy. *eLife.* 5:e09347.

75. Hyman, A. A., C. A. Weber, and F. Jülicher. 2014. Liquid-liquid phase separation in biology. *Annu. Rev. Cell Dev. Biol.* 30:39–58.

Biophysical Journal, Volume *112*

Supplemental Information

Volume Transitions of Isolated Cell Nuclei Induced by Rapid Temperature Increase

Chii J. Chan, Wenhong Li, Gheorghe Cojoc, and Jochen Guck

SUPPLEMENTARY MATERIAL

Volume transitions of isolated cell nuclei in response to rapid temperature increase
by C. J. Chan *et al.*

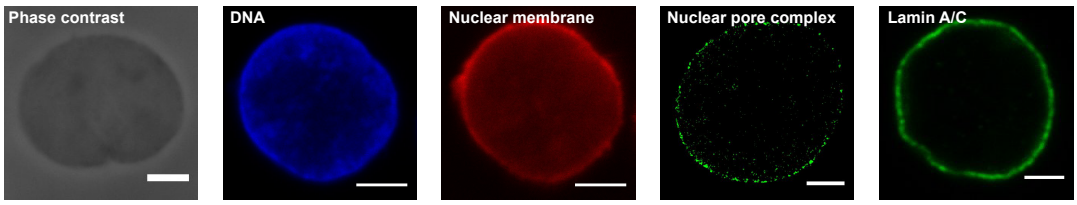

Fig. S1: Images of nuclear components in swollen state. Phase contrast and confocal images of isolated HL60 nuclei stained for DNA (Hoechst), membrane (FM4-64), nuclear pore complex (Mab414) and lamin A/C (anti-lamin A/C), in deionized water. Chromatin in DI appeared more decondensed than those in PBS, and preferentially located at the nuclear periphery. The nuclear pore complex (NPC) are preserved in the swollen state, as shown by the punctuated rim at the nuclear membrane. The NPCs appeared more sparsely distributed in swollen nuclei than those in PBS (see **Fig. 1a** in main text). Overall, the existence of a nuclear membrane, lamin and NPC indicate that the nuclear envelope for HL60 nuclei is intact even when heavily swollen. Scale bars 5 μm.

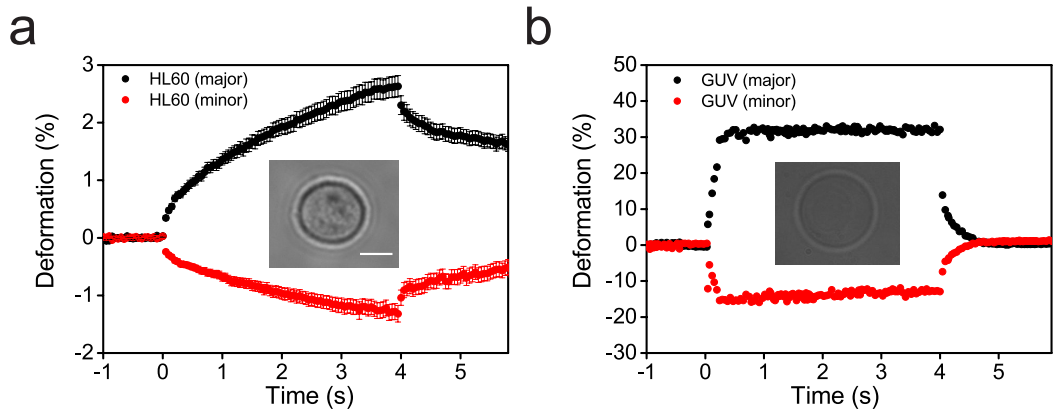

Fig. S2: Volume conservation for cells and giant unilamellar vesicles (GUVs) upon optical stretching in 780 nm OS in PBS prepared in deionized water. Average deformation profiles for **a**. HL60 cells (n = 54) and **b.** a representative GUV. Stretch power = 1.6 W, $\Delta T_{laser} \approx 3°C$. Negative deformation along minor axis (red) is approximately half that of the positive deformation along the major axis (black) in both cases, indicating volume conservation. HL60 cells showed more viscoelastic creep response while the GUVs appeared more elastic, which is also characterized by the immediate relaxation at the end of the stretch. Stretch period is from t = 0 to 4 s. Error bars represent SE. Scale bar 5 μm.

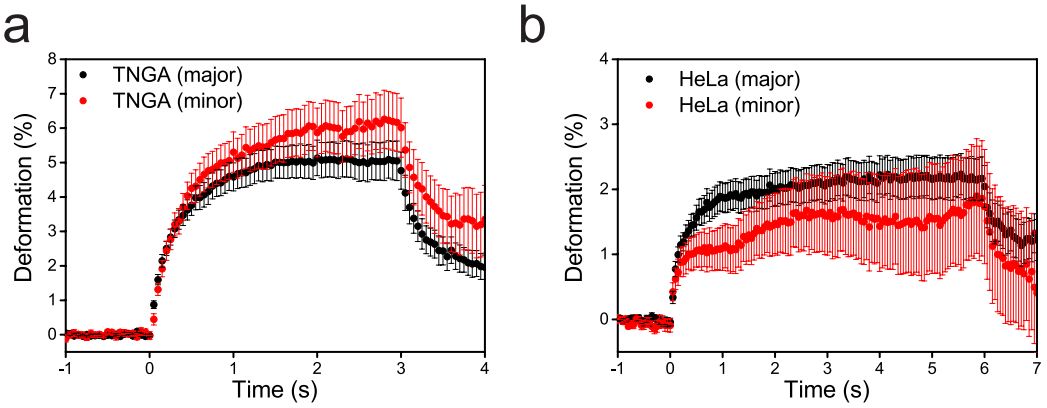

Fig. S3: Nuclear swelling in other cell types upon optical stretching in 1064 nm OS. a. Deformation curves for isolated TNGA mouse embryonic stem cell nuclei (n = 24), when stretched under 2.0 W ($\Delta T_{laser} \approx 22°C$), with stretch period from t = 0 to 3 s. **b**. Deformation curves for isolated HeLa nuclei (n = 60), when stretched with 1.4 W ($\Delta T_{laser} \approx 15°C$) between t = 0 to 6 s. Error bars represent SE.

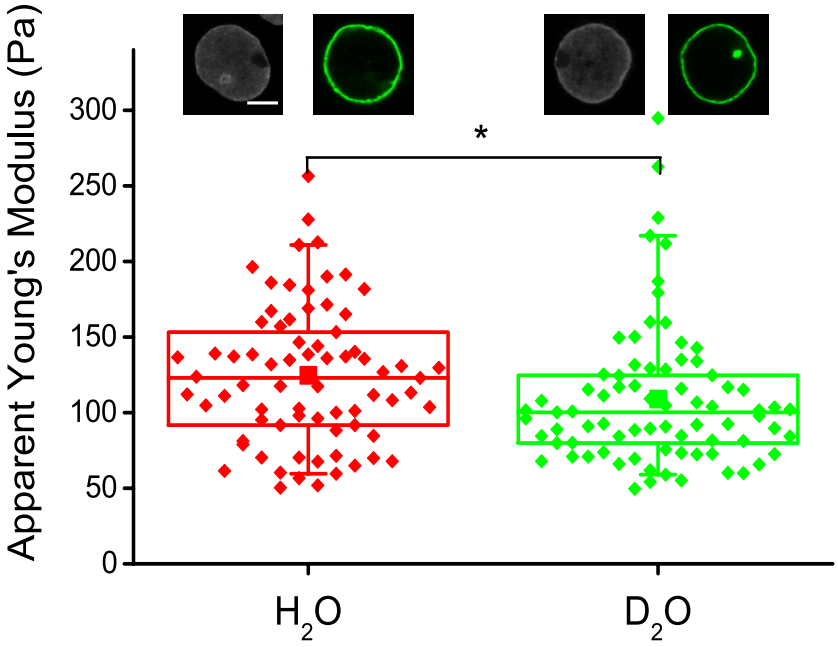

Fig. S4: AFM measurements of HL60 nuclei in 20%PBS prepared in heavy (D_2O) and deionized water (H_2O). There is only a minor difference (*$p < 0.05$) of the apparent Young's moduli between nuclei prepared with heavy water (n = 77) and deionized water (n = 73), suggesting that heavy water does not significantly change the nuclear stiffness. If any, they led to a slight reduction in nuclear stiffness, opposite to findings from OS studies. Inset depicts images of nuclei stained with DNA (grey) and lamin A/C (green), showing no visible difference in morphology and size of nuclei in heavy and deionized water. Scale bar 5 μm.

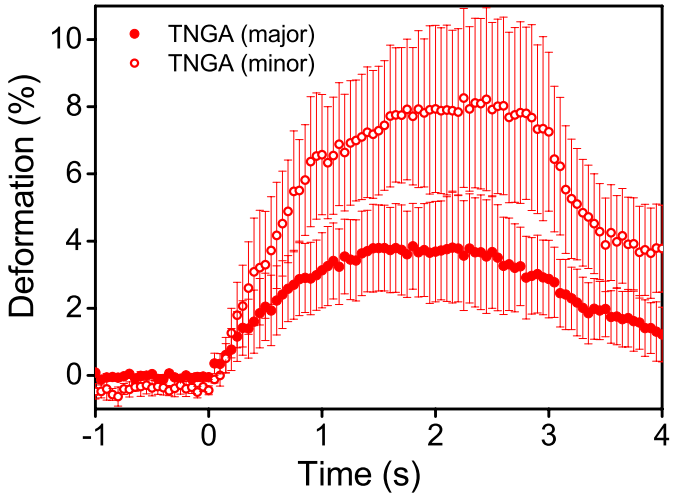

Fig. S5: Nuclear swelling upon laser heating by 1480 nm laser. TNGA nuclei (n = 16) in PBS were trapped by the 1064 nm OS and heated by a 1480 nm diode laser coupled to one of the 1064 nm optical fibers. Heating period is from t = 0 to 3 s. Error bars represent SE.

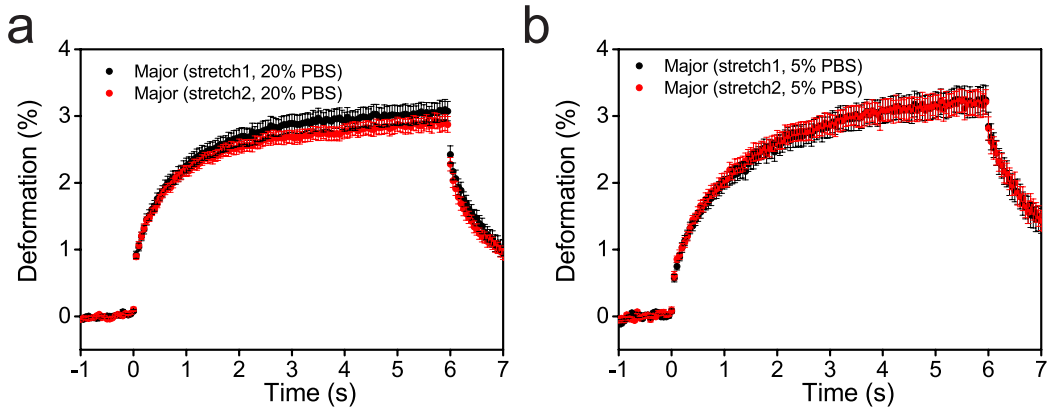

Fig. S6: Repeat heating experiments on HL60 nuclei in 780 nm OS. Major deformation profiles for HL60 nuclei in 20% PBS (**a**, n = 108) and 5% PBS (**b**, n = 108), during the first (black) and second stretch (red). Stretch periods are from t = 0 to 6 s. Both are prepared in deionized water, but heating is still minimal in the 780 nm OS (stretch power = 1.6 W, $\Delta T_{laser} \approx 3°C$). The deformation profiles overlap with each other indicating that the TIVT is highly reversible with no visible hysteresis. Error bars represent SE.

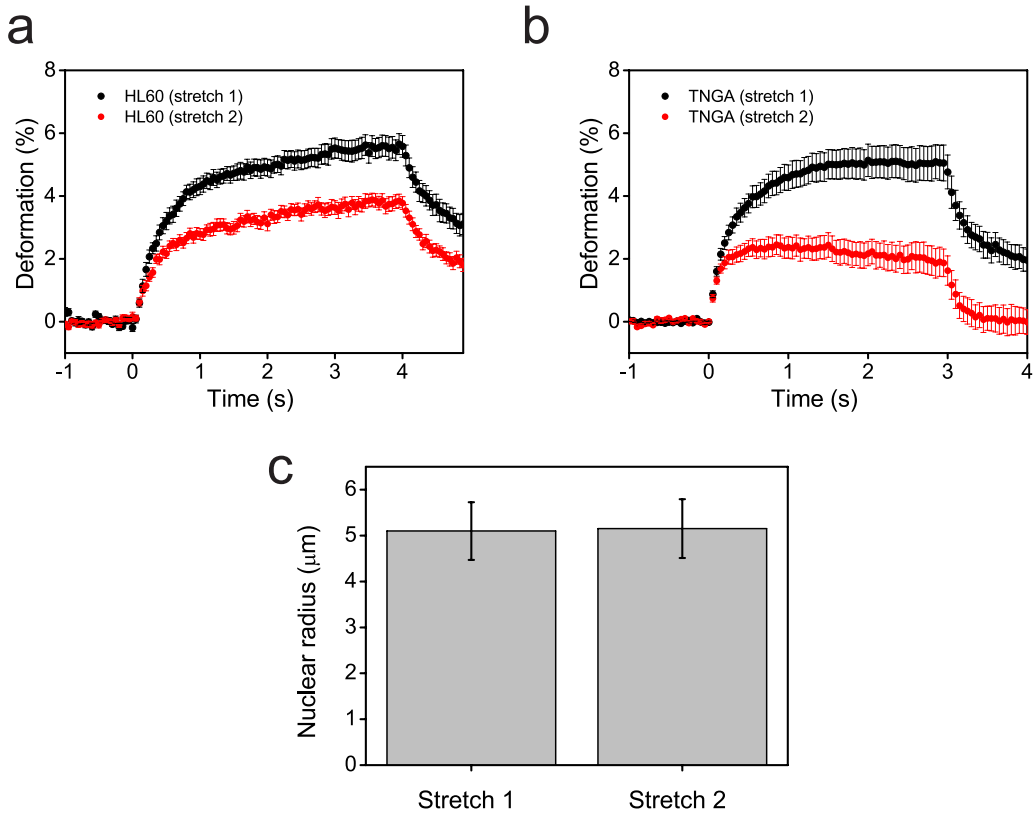

Fig. S7: Repeat heating experiments on isolated nuclei in 1064 nm OS. Deformation profiles along the major axis, for **a**. HL60 nuclei (n = 32, heating period t = 0 to 4 s), and **b**. TNGA nuclei (n = 18, heating period t = 0 to 3 s) during the first (black) and second stretch (red). Heating was more pronounced (stretch power = 1.6 W, $\Delta T_{laser} \approx 18°C$). **c**. Comparison of the initial nuclear size before the start of each stretch. The lack of a difference in the initial size suggests that the reduced amount of TIVT is not due to incomplete relaxation of nuclei and nuclear pre-strain before the next stretch. Error bars denote SE.

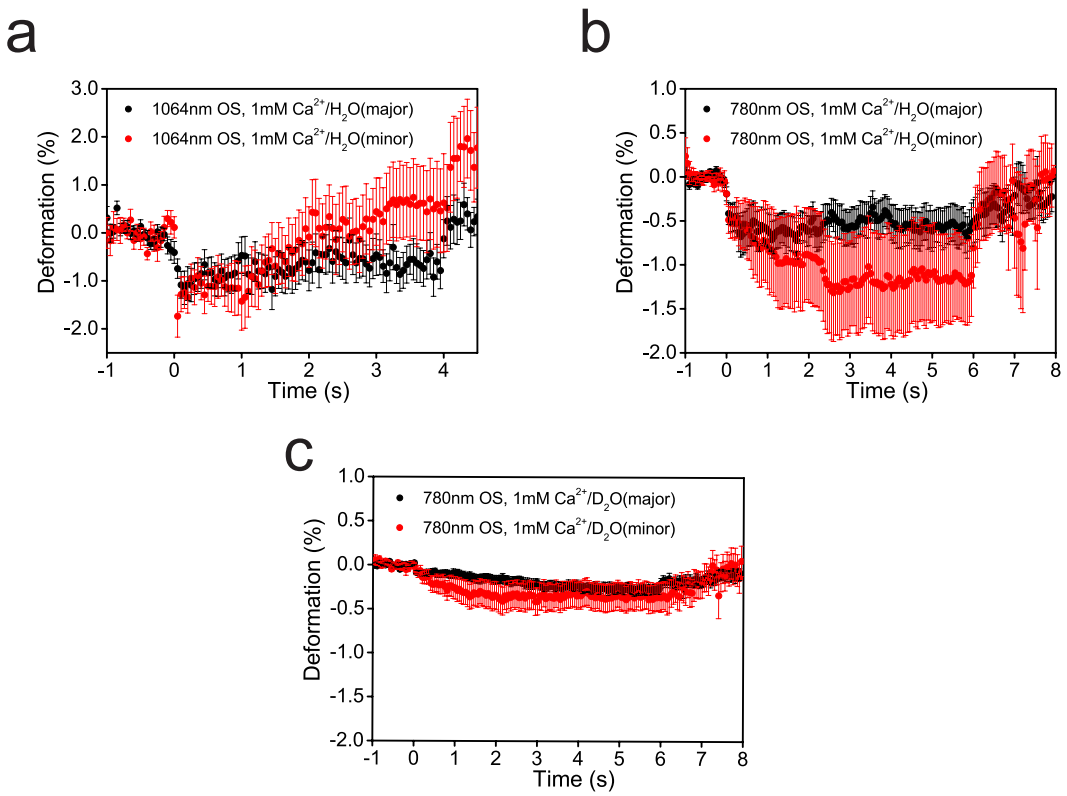

Fig. S8: Temperature induced nuclear contraction in multivalent salts correlates with the amount of transient heat. Deformation profiles for HL60 nuclei in **a.** 1 mM of $CaCl_2$ under optical stretching in 1064 nm OS (n = 17, $\Delta T_{laser} \approx 18°C$, stretch period t = 0 to 4 s), **b.** 1 mM of $CaCl_2$ (deionized water) in 780 nm OS (n = 17, $\Delta T_{laser} \approx 3°C$, stretch period t = 0 to 6 s), and **c.** 1 mM of $CaCl_2$ (heavy water) in 780 nm OS (n = 89, $\Delta T_{laser} \approx 1°C$, stretch period t = 0 to 6 s). Contraction along both axes is less pronounced with decreased laser-induced heating. Error bars denote SE.

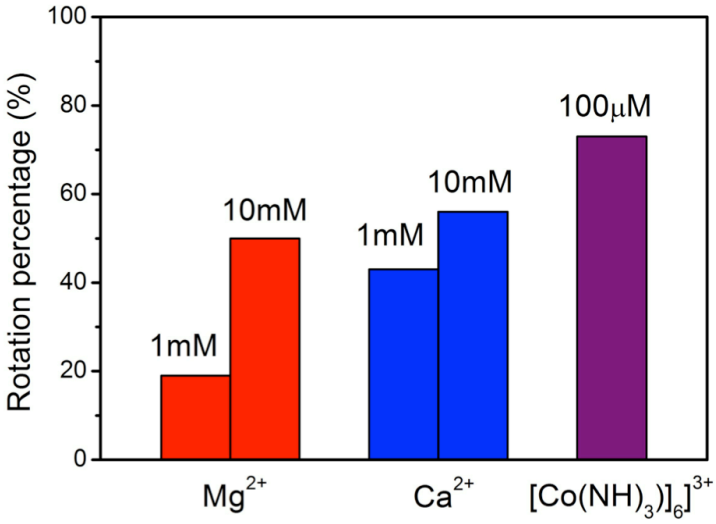

Fig. S9: Rotation statistics of nuclei under optical stretching in various multivalent salt concentrations. Higher concentrations of multivalent salts led to more nuclear rotations, with higher valency ions exerting a stronger effect. More than 30 nuclei are analyzed for each experimental condition.

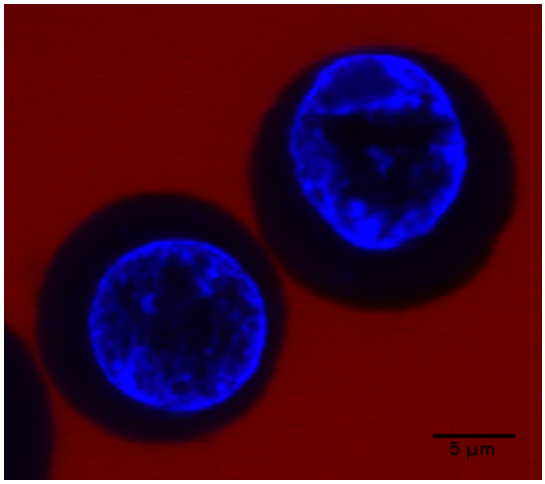

Fig. S10: Chromatin distribution in HL60 cells. Confocal composite image of HL60 cells stained for nucleus (Hoechst, blue) in PBS filled with rhodamine labeled 70 kDa (red) dextran. Pronounced compartmentalization of chromatin to the nuclear periphery was observed *in situ*, similar to those observed in isolated HL60 nuclei *in vitro*.

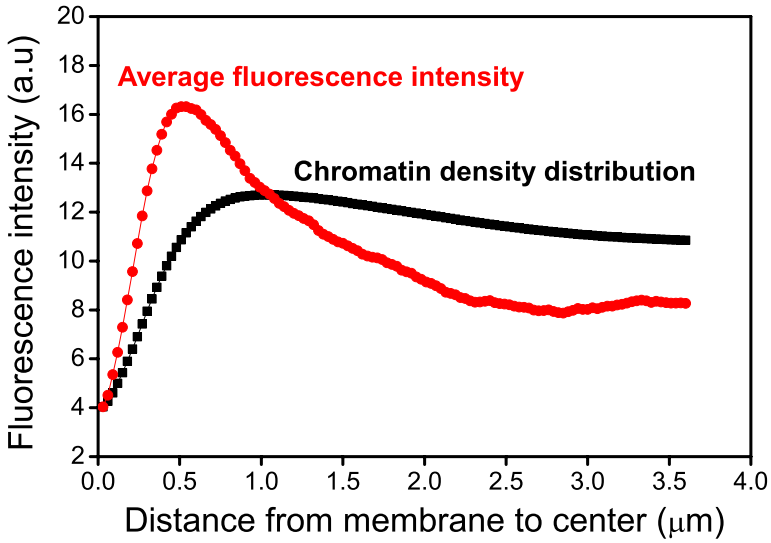

Fig. S11: Quantification of cortical chromatin distribution via fluorescence intensity profile analysis. The plots depict representative profiles (single nucleus) of the average fluorescence intensity and integrated intensity versus distance from the nuclear membrane to the center of the nucleus.

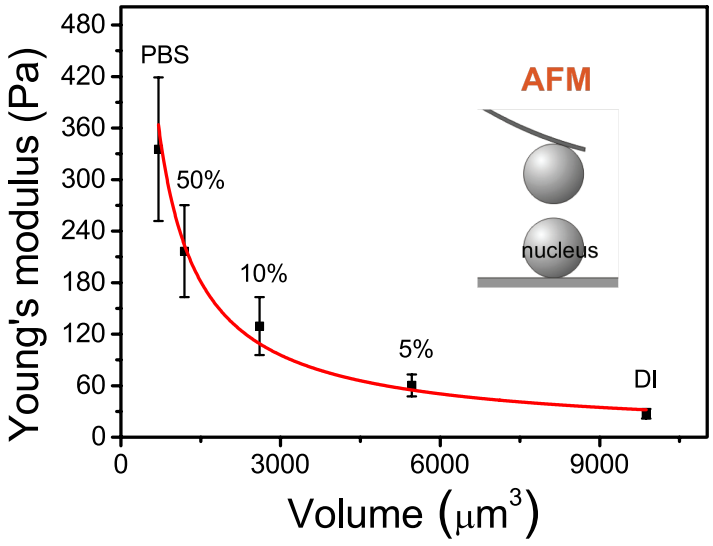

Fig. S12: AFM measurements of cortical chromatin stiffness for HL60 nuclei. Apparent stiffness of isolated HL60 nuclei swollen to various sizes, measured by AFM. Error bars denote SD. The measured values of the average Young's moduli are 335.4 ± 83.6 Pa, 216.7 ± 53.7 Pa, 129.4 ± 33.8 Pa, 60.3 ±12.7 Pa, and 27.4 ± 5.6 Pa for nuclei in PBS, 50% PBS, 10% PBS, 5% PBS and deionized water, respectively. The red curve denotes a fit based on the allometric model: $E = 1.7 \times 10^5 V^{-0.938}$ Pa. Adjusted goodness of fit $R^2 = 0.957$ indicates a good agreement with the measured data. More than 50 nuclei were analysed for each data point.

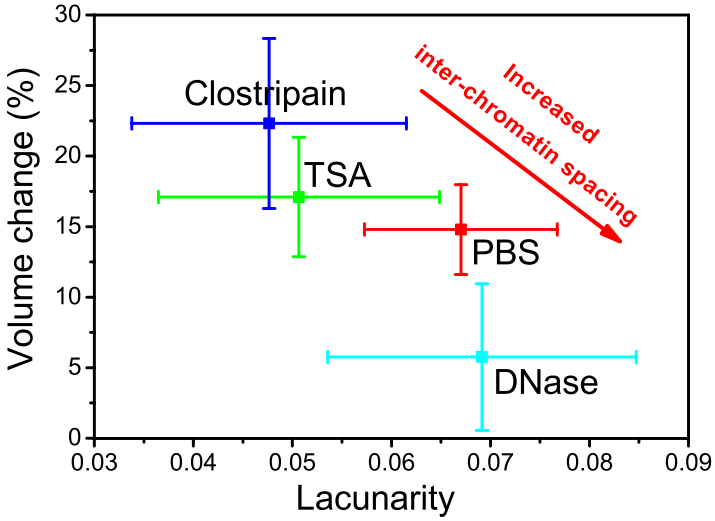

Fig. S13: Temperature-induced volume changes of nuclei versus lacunarity under pharmacological treatments. Lacunarity measures the texture and the distribution of voids in an image. Higher lacunarity indicates more voids or 'gappiness' in the image. The lacunarity of the nucleus significantly decreased under histone modifications (TSA, $n = 44$) and proteolysis (clostripain, $n = 27$), indicating that chromatin decondensation leads to a shrinkage of the pores and channels interdigitating the chromatin domains. Nuclei in PBS ($n = 21$) and DNase ($n = 17$), on the other hand, revealed higher lacunarity indicating uneven distribution of chromatin punctuated by dark, chromatin-free pores. Error bars denote SD.

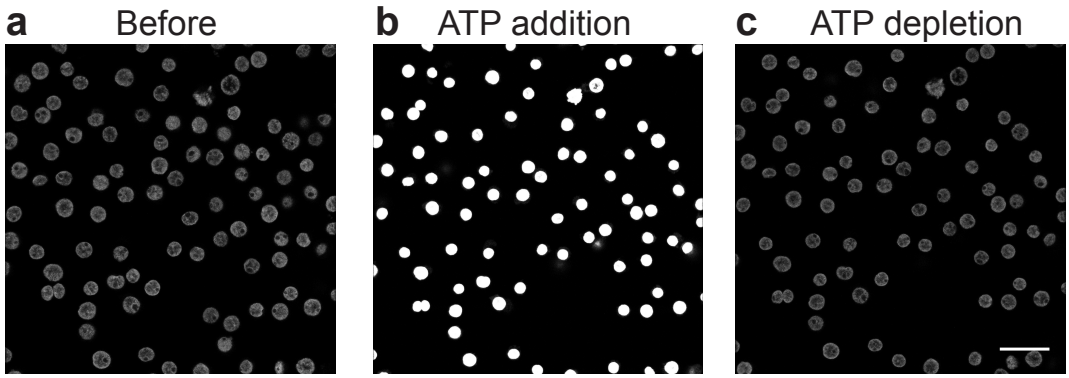

Fig. S14: Reversibility of chromatin condensation state induced by ATP. Confocal images of Hoechst stained HL60 nuclei in PBS buffer (**a**), followed by addition of ATP (**b**), which induces chromatin compaction and nuclear stiffening. Subsequent ATP depletion (**c**) further decondenses the chromatin, which correlates with nuclear softening against TIVT during optical stretching. Data was collected with identical microscope settings. Scale bar denotes 40 μm.

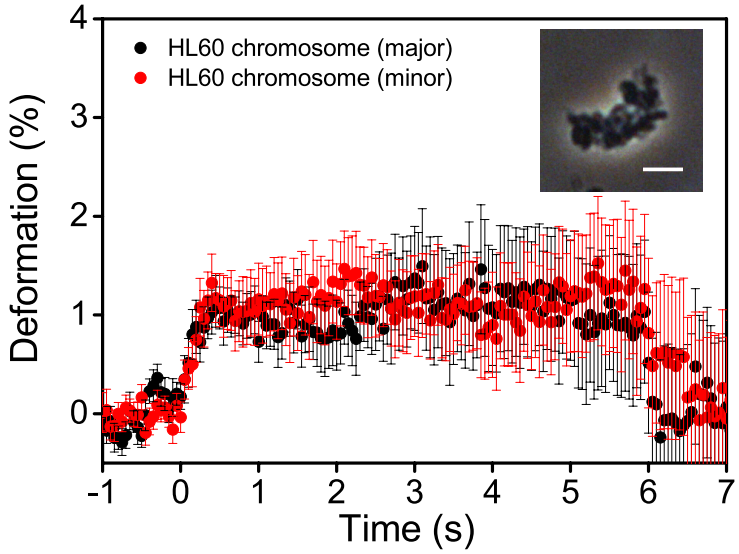

Fig. S15: HL60 mitotic chromosomes exhibit swelling under optical stretching in 1064 nm OS. Deformation curves for isolated HL60 chromosomes (n = 34), when stretched with 2.0 W ($\Delta T_{laser} \approx 23°C$) between t = 0 and 6 s. Inset depicts a phase contrast image of isolated chromosome. Error bars denote SE. Scale bar 5 μm.

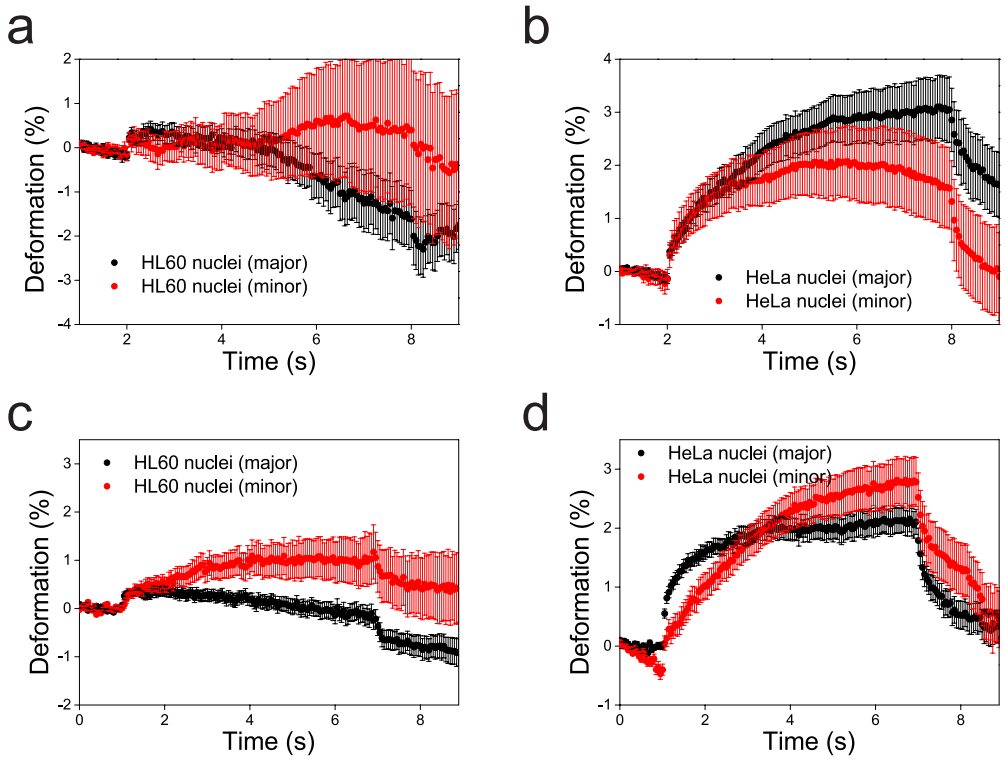

Fig. S16: Nuclear deformation *in situ* in OS. Nuclear deformation for a) HL60 (n = 31) and b) HeLa cells (n = 61), in an 1064 nm OS ($\Delta T_{laser} \approx 22°C$). Similar nuclear deformation profiles were observed for c) HL60 (n = 42) and d) HeLa nuclei (n = 51) *in situ* when stretched in an 780 nm OS in PBS prepared in D_2O ($\Delta T_{laser} \approx 1°C$).

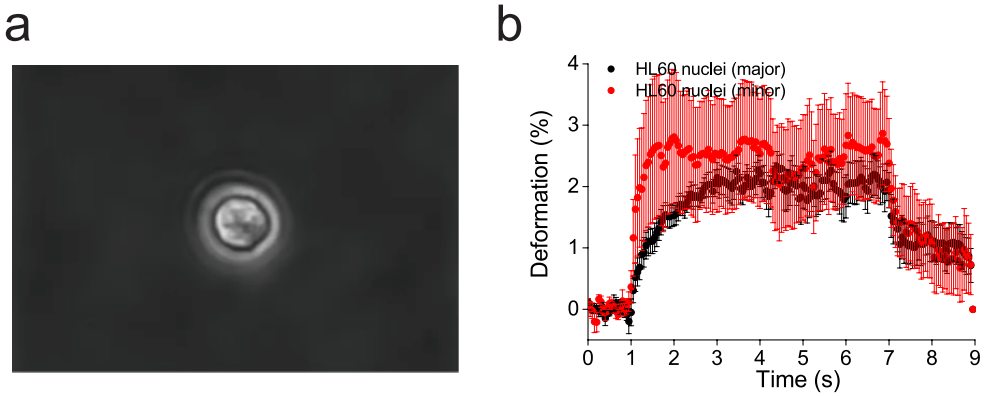

Fig. S17: a) Phase contrast image of isolated HL60 nuclei in 35 kDa PEG solution, under optical heating in 780nm OS. b) Average deformation profiles for a), when the nuclei (n = 11) are stretched with a total power of 1.6W and $\Delta T_{laser} \approx 3°C$. Stretch period is between t = 1 to 7 s. Error bars represent SE.

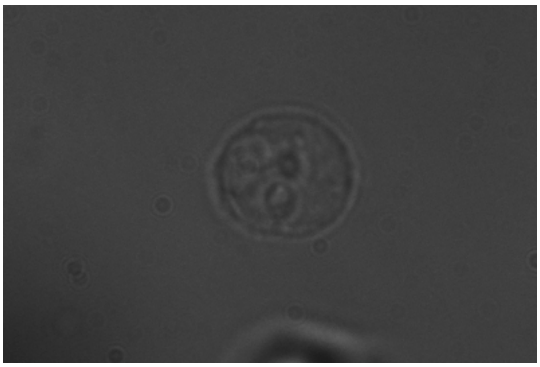

Movie. S1: Nuclear swelling in monovalent salts under optical stretching. Isolated HL60 nuclei swell in the presence of 100 mM of NaCl during TIVT. Laser power = 1.6 W, $\Delta T_{laser} \approx 18°C$. (WMV)

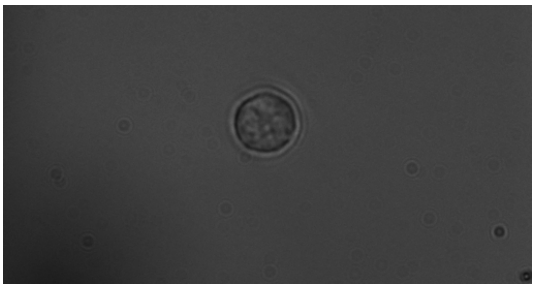

Movie. S2: Nuclear contraction in high concentrations of multivalent salts under optical stretching. Isolated HL60 nuclei contract in the presence of 10 mM of $MgCl_2$ during TIVT. Laser power = 1.6 W, $\Delta T_{laser} \approx 18°C$. (WMV)

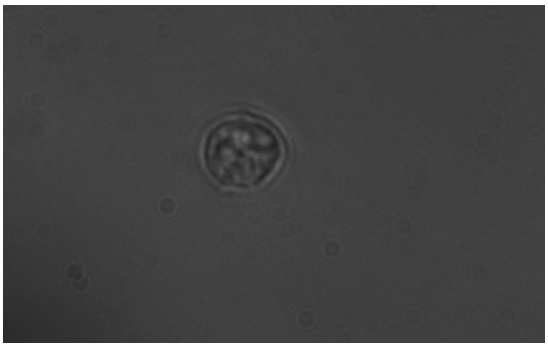

Movie. S3: Nuclear rotation in high concentrations of multivalent salts under optical stretching. Isolated HL60 nucleus can exhibit rotation along the major axis in 10 mM of $CaCl_2$ during TIVT. Laser power = 1.6 W, $\Delta T_{laser} \approx 18°C$. (WMV)